

# Beamforming Design with Partial Channel Estimation and Feedback for FDD RIS-Assisted Systems

Xiaochun Ge, Shanping Yu, Wenqian Shen, Chengwen Xing, *Member, IEEE*, and  
Byonghyo Shim, *Senior Member, IEEE*

## Abstract

Beamforming design with partial channel estimation and feedback for frequency-division duplexing (FDD) reconfigurable intelligent surface (RIS) assisted systems is considered in this paper. We leverage the observation that path angle information (PAI) varies more slowly than path gain information (PGI). Then, several dominant paths are selected among all the cascaded paths according to the known PAI for maximizing the spectral efficiency of downlink data transmission. To acquire the dominating path gain information (DPGI, also regarded as the path gains of selected dominant paths) at the base station (BS), we propose a DPGI estimation and feedback scheme by jointly beamforming design at BS and RIS. Both the required number of downlink pilot signals and the length of uplink feedback vector are reduced to the number of dominant paths, and thus we achieve a great reduction of the pilot overhead and feedback overhead. Furthermore, we optimize the active BS beamformer and passive RIS beamformer by exploiting the feedback DPGI to further improve the spectral efficiency. From numerical results, we demonstrate the superiority of our proposed algorithms over the conventional schemes.

## Index Terms

Reconfigurable intelligent surface, FDD, path selection, feedback reduction, active and passive beamforming

X. Ge, W. Shen, and C. Xing are with School of Information and Electronics, Beijing Institute of Technology, Beijing 100081, China (e-mail: xiaochun\_ge\_bit\_ee@163.com; shenwq@bit.edu.cn; xingchengwen@gmail.com).

S. Yu is with the School of Cyberspace Science and Technology, Beijing Institute of Technology, Beijing 100081, China (e-mail: ysp@bit.edu.cn).

B. Shim is with the Institute of New Media and Communications, Department of Electrical and Computer Engineering, Seoul National University, Seoul 08826, South Korea (e-mail: bshim@snu.ac.kr).

## I. INTRODUCTION

### A. Motivation

Recently, reconfigurable intelligent surfaces (RISs) (also known as intelligent reflecting surfaces, IRSs) have been envisioned as a promising technique for the beyond fifth-generation (B5G) and sixth-generation (6G) wireless communication systems due to their potential to smartly reconfigure the wireless propagation environment in an energy-efficient and environment-friendly manner [1]–[3]. RISs are nearly-passive devices composed of arrays of reflecting elements which can reconfigure the incident signals [4]. Specifically, if the channel state information (CSI) is perfectly known, the quality of wireless communication can be improved by adjusting the RIS reflection coefficients with the aid of a centralized controller [5]. Therefore, the optimization of RIS reflection coefficients has been widely studied under different setups [6], [7], where the effectiveness of RIS in achieving high spectral efficiency with low energy and hardware cost is verified [5], [8], [9].

To fully exploit the potential of RIS-assisted communication systems, the centralized controller needs to acquire the CSI accurately [10], so most of the aforementioned literatures mainly assume the perfect CSI is available [11]. However, the acquisition of CSI is very challenging in practice. In the widely used time-division duplexing (TDD) systems, downlink CSI can be acquired by the uplink channel estimation according to the channel reciprocity between the uplink and downlink wireless channels [12]–[15].<sup>1</sup> Hence, existing works mainly consider the channel estimation problems in TDD RIS-assisted systems [16]–[21]. In practice, however, considering the difference between radio frequency (RF) circuits of the transmitting branch and the receiving branch, the required accuracy of antenna array calibration to maintain the channel reciprocity in TDD mode is extremely high [22]. Therefore, it is of importance to come up with the design and optimization of RIS-assisted systems for the widely used frequency-division duplexing (FDD) mode, where the uplink and downlink channels are operated at different frequency bands [23].

Since the channel reciprocity no longer holds in FDD systems, downlink CSI should be estimated using downlink pilot signals at the user equipment (UE) and then fed back to the base station (BS). However, the overhead of directly feeding back the downlink CSI is unaffordable

<sup>1</sup>The experimental results in [12] validate that the channel reciprocity holds in RIS-assisted TDD systems as long as the employed RISs are commonly designed and fabricated, and conform to the prerequisite of the Rayleigh-Carson reciprocity theorem, which has been discussed in detail in [12].

in practice, especially for RIS-assisted systems with an extremely large number of RIS elements [24]. Although there is no path gain reciprocity between the uplink and downlink channels in FDD RIS-assisted systems, it is pointed out that angle reciprocity (i.e. the angles of paths are quite similar in the uplink and downlink channels) still holds [12], [25]. Therefore, in order to effectively reduce the feedback overhead in FDD RIS-assisted systems, we focus on estimating and feeding back the path gain information (PGI), while the path angle information (PAI) can be obtained via the angle reciprocity [12]. Furthermore, motivated by [26], we select several paths as dominant paths, and then estimate and feed back their corresponding dominating path gain information (DPGI) to further reduce pilot overhead and feedback overhead.

### *B. Related Work*

Over the years, various channel estimation techniques for the RIS-assisted systems have been proposed [16]–[21]. In [16] and [21], utilizing the sparse property of millimeter wave (mmWave) channels [27], [28], the compressive sensing (CS) based estimator and the alternating direction method of multipliers (ADMM) based estimator have been proposed, where both of which estimate the cascaded channel with a low training overhead. In [17], a two-step channel estimation approach exploiting the common row-column-block sparsity structure among the uplink channel matrices of all users has been proposed. Although the aforementioned works [16]–[21] mainly consider the channel estimation problems for TDD mode, the estimators proposed can be easily extended or effectively applied to PAI acquisition at BS for FDD mode [23].

Existing works focused on FDD RIS-assisted networks are relatively limited (see, e.g. [13], [23], [24], [29]–[33]). Specifically, to avoid the performance degradation in practical application of RIS-assisted systems, the authors in [29] and [30] discussed the downlink channel tracking and the optimization of phase shifts at RIS, respectively. Moreover, a two-way passive RIS beamforming design has been proposed in [31], where the passive beamformers for downlink and uplink are optimized simultaneously. Besides, the authors in [32] further extended the reflecting beamforming design to multi-user scenarios, which effectively shows the great potential of RIS in FDD systems. In addition, we note that the system performance of FDD RIS-assisted networks is often limited by the unaffordable CSI feedback overhead. In [13] and [23], the similarity among the RIS-UE channels of all users is exploited to reduce the CSI feedback overhead. The authors in [24] designed a cascaded codebook for the feedback of PGI by assuming that downlink CSI (including both PAI and PGI) is perfectly known at UE, and further carried out an in-depth study

for multi-RIS-assisted systems in [33]. On this basis, we turn to consider the feedback of DPGI with a smaller dimension (rather than the whole PGI) by selecting several dominant paths to further reduce the feedback overhead, and the DPGI estimation scheme with low pilot overhead is also provided.

### C. Main Contributions

In this paper, we propose a path selection technique with reduced pilot overhead and feedback overhead as well as a partial CSI-based beamforming design for the FDD RIS-assisted wireless communication systems. Our main contributions are summarized as follows:

- We propose a path selection strategy for the FDD RIS-assisted systems. It is observed that PAI varies more slowly than PGI, so PAI can be considered as unchanged and acquired by BS during a relatively long time named ‘angle coherence time’ [34]. Hence, we calculate the contributions of all the cascaded paths to the spectral efficiency based on PAI, and remove the path with minimal contribution sequentially, where the active and passive beamformers are optimized alternatively. Then, the remaining paths and their corresponding PGI are regarded as selected dominant paths and DPGI, respectively. In this way, the dimension of vector (corresponding to DPGI) to be estimated and fed back are effectively reduced without significant performance degradation.
- We propose a DPGI estimation and feedback scheme by exploiting PAI known at BS according to the angle reciprocity, where the accuracy of DPGI estimation is greatly improved by jointly designing the active BS beamforming and passive RIS beamforming. In our proposed scheme, we set the required number of downlink training pilot signals and the length of uplink feedback vector to the number of dominant paths. Therefore, we achieve a great reduction of the pilot and feedback overhead over the existing least square (LS)-based and minimum mean-square error (MMSE)-based estimators [21].<sup>2</sup>
- We propose an algorithm to alternatively update the active and passive beamformers on the basis of fed back DPGI for further improving the spectral efficiency of downlink data transmission. Moreover, numerical results of the proposed schemes together with several conventional schemes are provided, from which we demonstrate the superiority of proposed algorithms in system performance, required pilot signals and feedback overhead.

<sup>2</sup>The number of pilot signals required for LS-based estimator and MMSE-based estimator is often on the order of the number of BS antennas/RIS elements [35].

### D. Paper Outline

The rest of this paper is organized as follows. The system model of the RIS-assisted mmWave communications is presented in Section II. Then, the path selection technique, DPGI estimation and feedback scheme, and beamforming design are proposed in Section III. Simulation results are provided in Section IV. Finally, we conclude our work in Section V.

### E. Notation

In this paper, lower-case and boldface capital letters represent column vectors and matrices, respectively. Besides, We denote  $(\cdot)^*$ ,  $(\cdot)^T$ ,  $(\cdot)^H$ ,  $|\cdot|$ ,  $\|\cdot\|$ ,  $\|\cdot\|_F$ ,  $(\cdot)^{-1}$ ,  $\Re\{\cdot\}$ ,  $\mathbb{E}\{\cdot\}$ , and  $\text{Tr}\{\cdot\}$  as the conjugate, transpose, conjugate transpose, determinant of a matrix/absolute value of a scalar/cardinality of a set, Euclidean norm of a vector, Frobenius norm of a matrix, inverse, real part, statistical expectation, and trace operators, respectively.  $\text{vec}\{\cdot\}$  denotes the vectorization of a matrix (i.e. a linear transformation which stacks the columns of a matrix on top of one another to obtain a column vector), and  $\text{invec}\{\cdot\}$  denotes the inverse of vectorization. The Hadamard product and Kronecker product are denoted by  $\odot$  and  $\otimes$ . In addition, all 0 matrix and all 1 matrix with dimension of  $M \times N$  are represented by  $\mathbf{0}_{M \times N}$ , and  $\mathbf{1}_{M \times N}$ , respectively, and  $\mathbf{I}_M$  denotes an identity matrix of size  $M \times M$ .  $\mathbf{X}^{i,j}$  denotes the  $(i, j)$ -th element of matrix  $\mathbf{X}$ . Finally,  $\mathcal{CN}(\mathbf{0}, \mathbf{R})$  denotes the zero-mean complex Gaussian distribution with covariance matrix  $\mathbf{R}$ .

## II. SYSTEM MODEL

In this section, we discuss the signal model of the RIS-assisted mmWave wireless communications and the angle reciprocity for the FDD RIS-assisted systems. We then explain the channel feedback mechanism for the FDD RIS-assisted wireless communication systems.

### A. RIS-assisted mmWave Wireless Communication Model

In this paper, an RIS-assisted mmWave wireless communication system is investigated. Since the direct BS-UE channel has been studied extensively in many previous works and blockage is a critical issue for mmWave wireless communications, we consider the case without a direct link between BS and a single-antenna UE [23]. This means that an RIS is used to improve the quality of wireless communication. Through an RIS controller, BS can control the RIS to manipulate the electromagnetic response of incident waves. In our work, uniform planar arrays (UPAs) are equipped at both BS and RIS. By using the subscript ‘v’ for vertical system parameters and the

subscript ‘h’ for horizontal system parameters, the number of BS antennas and RIS elements can be expressed as  $N_B = N_{B,v} \times N_{B,h}$  and  $N_R = N_{R,v} \times N_{R,h}$ . The cascaded channel vector  $\mathbf{h} \in \mathbb{C}^{N_B \times 1}$  between BS and UE is

$$\mathbf{h}^H = \mathbf{h}_{RU}^H \Psi \mathbf{H}_{RB}, \quad (1)$$

where  $\mathbf{H}_{RB} \in \mathbb{C}^{N_R \times N_B}$  and  $\mathbf{h}_{RU} \in \mathbb{C}^{N_R \times 1}$  denote the BS-RIS channel matrix and the RIS-UE channel vectors. The reflection coefficient matrix of RIS can be expressed as

$$\Psi = \text{diag}(\boldsymbol{\psi}) = \text{diag}([e^{j\psi_1}, e^{j\psi_2}, \dots, e^{j\psi_{N_R}}]^T) \in \mathbb{C}^{N_R \times N_R}. \quad (2)$$

According to the sparsity of mmWave channel,  $\mathbf{H}_{RB}$  can be expressed as the sum of several propagation paths, which is given by [10], [27]

$$\mathbf{H}_{RB} = \sqrt{\frac{N_B N_R}{L_{RB}}} \mathbf{A}_{RB} \text{diag}(\boldsymbol{\alpha}) \mathbf{A}_B^H \in \mathbb{C}^{N_R \times N_B}, \quad (3)$$

where  $L_{RB}$  and  $\boldsymbol{\alpha} = [\alpha_1, \alpha_2, \dots, \alpha_{L_{RB}}]^T \in \mathbb{C}^{L_{RB} \times 1}$  denote the number of paths in BS-RIS channel and the normalized complex gain with  $\alpha_p \sim \mathcal{CN}(0, 1)$  for  $p = 1, 2, \dots, L_{RB}$ .

Similarly,  $\mathbf{h}_{RU}^H$  is given by

$$\mathbf{h}_{RU}^H = \sqrt{\frac{N_R}{L_{RU}}} \boldsymbol{\beta}^T \mathbf{A}_{RU}^H \in \mathbb{C}^{1 \times N_R}, \quad (4)$$

where  $L_{RU}$  and  $\boldsymbol{\beta} = [\beta_1, \beta_2, \dots, \beta_{L_{RU}}]^T \in \mathbb{C}^{L_{RU} \times 1}$  are the number of paths in RIS-UE channel and the normalized complex gain with  $\beta_q \sim \mathcal{CN}(0, 1)$ , for  $q = 1, 2, \dots, L_{RU}$ . Furthermore,  $\mathbf{A}_B = [\mathbf{a}_{B,1}, \mathbf{a}_{B,2}, \dots, \mathbf{a}_{B,L_{RB}}] \in \mathbb{C}^{N_B \times L_{RB}}$ ,  $\mathbf{A}_{RB} = [\mathbf{a}_{RB,1}, \mathbf{a}_{RB,2}, \dots, \mathbf{a}_{RB,L_{RB}}] \in \mathbb{C}^{N_R \times L_{RB}}$ , and  $\mathbf{A}_{RU} = [\mathbf{a}_{RU,1}, \mathbf{a}_{RU,2}, \dots, \mathbf{a}_{RU,L_{RU}}] \in \mathbb{C}^{N_R \times L_{RU}}$  are the transmitting array response matrix at BS, the receiving array response matrix at RIS and the transmitting array response matrix at RIS, respectively. For  $p = 1, 2, \dots, L_{RB}$  and  $q = 1, 2, \dots, L_{RU}$ , we have

$$\mathbf{a}_{B,p} = \mathbf{a}_v(N_{B,v}, \theta_{B,v,p}) \otimes \mathbf{a}_h(N_{B,h}, \theta_{B,v,p}, \theta_{B,h,p}) \in \mathbb{C}^{N_B \times 1}, \quad (5)$$

$$\mathbf{a}_{RB,p} = \mathbf{a}_v(N_{R,v}, \phi_{RB,v,p}) \otimes \mathbf{a}_h(N_{R,h}, \phi_{RB,v,p}, \phi_{RB,h,p}) \in \mathbb{C}^{N_R \times 1}, \quad (6)$$

$$\mathbf{a}_{RU,q} = \mathbf{a}_v(N_{R,v}, \theta_{RU,v,q}) \otimes \mathbf{a}_h(N_{R,h}, \theta_{RU,v,q}, \theta_{RU,h,q}) \in \mathbb{C}^{N_R \times 1}, \quad (7)$$

where the array response vectors of half-wavelength spaced UPAs are given by [24]

$$\mathbf{a}_v(N_v, \theta_v) = \sqrt{\frac{1}{N_v}} [1, e^{j\pi \cos(\theta_v)}, \dots, e^{j\pi(N_v-1) \cos(\theta_v)}]^T \in \mathbb{C}^{N_v \times 1}, \quad (8)$$

$$\mathbf{a}_h(N_h, \theta_v, \theta_h) = \sqrt{\frac{1}{N_h}} [1, e^{j\pi \sin(\theta_v) \sin(\theta_h)}, \dots, e^{j\pi(N_h-1) \sin(\theta_v) \sin(\theta_h)}]^T \in \mathbb{C}^{N_h \times 1} \quad (9)$$

with  $\theta_{B,v,p}$ ,  $\phi_{RB,v,p}$ , and  $\theta_{RU,v,q}$  ( $\theta_{B,h,p}$ ,  $\phi_{RB,h,p}$ , and  $\theta_{RU,h,q}$ ) denoting the angle of departure (AoD) of the  $p$ -th path for BS-RIS channel  $\mathbf{H}_{RB}$ , the angle of arrival (AoA) of the  $p$ -th path for BS-RIS channel  $\mathbf{H}_{RB}$  and the AoD of the  $q$ -th path for RIS-UE channel  $\mathbf{h}_{RU}$  in the vertical (horizontal) direction, respectively. Then, the channel vector in (1) can be rewritten as

$$\mathbf{h}^H = \sqrt{\frac{N_B N_R^2}{L}} \boldsymbol{\beta}^T \mathbf{A}_{RU}^H \boldsymbol{\Psi} \mathbf{A}_{RB} \text{diag}(\boldsymbol{\alpha}) \mathbf{A}_B^H, \quad (10)$$

where  $L = L_{RB} L_{RU}$  represents the total number of cascaded paths.

For the RIS-assisted wireless communication model, the downlink signal received at UE can be expressed as

$$y = \sqrt{P_t} \mathbf{h}^H \mathbf{f}_t s + n, \quad (11)$$

where  $P_t$  is the transmitting power,  $\mathbf{f}_t \in \mathbb{C}^{N_B \times 1}$  is the active beamformer at BS,  $s$  is the signal transmitted from BS satisfying  $\mathbb{E}[s s^*] = 1$ , and  $n \sim \mathcal{CN}(0, \sigma_n^2)$  is the complex Gaussian noise with noise power  $\sigma_n^2$ . Then, the achievable downlink spectral efficiency  $R$  is [26], [36]

$$R = \log_2 \left( 1 + \frac{P_t}{\sigma_n^2} \mathbb{E} \left[ |\mathbf{h}^H \mathbf{f}_t|^2 \right] \right). \quad (12)$$

### B. Angle Reciprocity for FDD RIS-assisted Systems

It is observed that only the signal components which physically reverse uplink propagation paths can be transmitted in the downlink for traditional FDD communication systems [26]. Hence, when the carrier frequencies between downlink and uplink channels do not differ too much, although their PGIs differ from each other, uplink PAI and downlink PAI are fairly similar, this phenomenon is often called angle reciprocity [26]. However, the introduction of RIS between BS and UE raises a question: are the uplink PAI and downlink PAI still similar? Fortunately, it can be proven that angle reciprocity still holds for the RIS-assisted wireless communications [12]. Therefore, BS can estimate the uplink PAI by using the pilot signals sent from UE, and then exploit the estimated PAI for the downlink beamforming design according to the angle reciprocity. In addition, channel estimation problems for the RIS-assisted systems have been widely studied (see, e.g. [16]–[18], [21]). Although many of them consider the TDD mode, the estimators can be easily extended or effectively applied to the acquisition of PAI at BS for the FDD mode [23], [37]. For example, according to the CS-based scheme in [21], the positions of cascaded paths can be calculated in the angular quantization grid, and then the estimate of PAI is acquired.

### C. Channel Feedback for FDD RIS-assisted Systems

In the FDD systems, the downlink CSI fed back from UE is essential for the beamforming design. The random vector quantization (RVQ) codebook is widely used for the CSI feedback. In this scheme, UE first normalizes the vector  $\mathbf{z} \in \mathbb{C}^{N \times 1}$  to be fed back as  $\bar{\mathbf{z}} = \frac{\mathbf{z}}{\|\mathbf{z}\|}$ , and then feeds back the codeword  $\hat{b}$  satisfying [34]

$$\hat{b} = \arg \max_{b \in \{1, 2, \dots, 2^B\}} |\bar{\mathbf{z}}^H \mathbf{c}_b|^2, \quad (13)$$

where  $\mathbf{C}_{\text{RVQ}} = [\mathbf{c}_1, \mathbf{c}_2, \dots, \mathbf{c}_{2^B}] \in \mathbb{C}^{N \times 2^B}$  is the pre-defined  $B$ -bits RVQ codebook with  $\|\mathbf{c}_b\|^2 = 1$  for  $b = 1, 2, \dots, 2^B$ .<sup>3</sup> To properly control the quantization distortion, the required number of feedback bits is given by  $B \approx \frac{(N-1)}{3} \times \text{SNR}$ , where SNR denotes the signal-to-noise-ratio for codeword transmission [26]. However, for a FDD RIS-assisted communication system with  $N_B$  antennas at BS and  $N_R$  reflecting elements at RIS, the overhead of directly feeding back downlink CSI (including both PAI and PGI) with dimension of  $N_B N_R \times 1$  is unbearable, which leads to an extremely huge number of feedback bits to achieve an acceptable feedback distortion [24]. Fortunately, downlink PAI can be acquired by the uplink channel estimation via the angle reciprocity and the slowly-varying characteristic of PAI. Then, only downlink PGI with dimension of  $L \times 1$  needs to be fed back. Thus, the dimension of feedback vector can be reduced from  $N_B N_R \times 1$  to  $L \times 1$ , where  $L = L_{\text{RB}} L_{\text{RU}}$  represents the total number of cascaded paths [24]. On this basis, inspired by [26], we choose a few dominant paths maximizing the spectral efficiency from all the cascaded paths, and feed back corresponding DPGI instead of the overall PGI to further reduce the feedback overhead in FDD RIS-assisted systems.

### III. PROPOSED PATH SELECTION BASED SCHEME

In this section, we present the path selection based feedback reduction and beamforming design scheme. The overall strategy and main steps are summarized in Fig. 1.

- *Step 1 (PAI acquisition)*: BS estimates the uplink PAI by using the pilot signals sent from UE and reflected by RIS (the feasibility of this step has been discussed in the aforementioned section, which will not be repeated in the following). According to the angle reciprocity of FDD systems, downlink PAI is equivalent to being acquired at BS.

<sup>3</sup>We follow the common assumption in channel feedback that the scalar  $\|\mathbf{z}\|$  (i.e. the magnitude of  $\mathbf{z}$ ) can be fed back perfectly, thereby the more challenging feedback of the vector  $\bar{\mathbf{z}}$  (i.e. the direction of  $\mathbf{z}$ ) is focused in this study [34].





According to (12), the spectral efficiency  $R$  can be improved by maximizing  $\mathbb{E} \left[ |\mathbf{h}^H \mathbf{f}_t|^2 \right]$ . Thus, we begin with rewriting the cascaded channel vector  $\mathbf{h} \in \mathbb{C}^{N_B \times 1}$  in (10) as

$$\mathbf{h} = \mathbf{A} \mathbf{g}^*, \quad (14)$$

where  $\mathbf{g} = \boldsymbol{\beta} \otimes \boldsymbol{\alpha} \in \mathbb{C}^{L \times 1}$  is the cascaded PGI. The matrix  $\mathbf{A}$  can be expressed as

$$\mathbf{A} = [\mathbf{a}_1, \mathbf{a}_2, \dots, \mathbf{a}_L] \in \mathbb{C}^{N_B \times L}, \quad (15)$$

$$\mathbf{a}_l = \mathbf{B}_l \boldsymbol{\psi}^* \in \mathbb{C}^{N_B \times 1}, \quad (16)$$

$$\mathbf{B}_l = \sqrt{\frac{N_B N_R^2}{L}} \mathbf{a}_{B,p} \mathbf{a}_{RB,p}^H \text{diag}(\mathbf{a}_{RU,q}) \in \mathbb{C}^{N_B \times N_R} \quad (17)$$

for  $l = 1, 2, \dots, L$ . The index  $l$  of cascaded paths is given by  $l = (q - 1)L_{RB} + p$  for  $p = 1, 2, \dots, L_{RB}$  and  $q = 1, 2, \dots, L_{RU}$ .

Initially, all the  $L$  paths are in the selected set. Then, the path with minimal contribution to  $R$  is removed sequentially until the number of remaining paths reaches the pre-defined number of dominant paths. In this iterative process, we denote  $L_s$  and  $\Lambda_s \subseteq \{1, 2, \dots, L\}$  as the number of remaining dominant paths and the set of corresponding indices satisfying  $|\Lambda_s| = L_s$ , where the indices in  $\{\Lambda_s\}$  are arranged in an ascending order. Similarly, the number of removed paths and the set of corresponding indices are denoted as  $L_r$  and  $\Lambda_r \subseteq \{1, 2, \dots, L\}$ , where  $L_r = L - L_s$ ,  $|\Lambda_r| = L_r$ , and the indices in  $\{\Lambda_r\}$  are also arranged in an ascending order. Thus, the cascaded channel in (14) can be decomposed as

$$\mathbf{h} = \mathbf{A}_s \mathbf{g}_s^* + \mathbf{A}_r \mathbf{g}_r^*, \quad (18)$$

where  $\mathbf{g}_s = [g_{s,1}, g_{s,2}, \dots, g_{s,L_s}]^T \in \mathbb{C}^{L_s \times 1}$  and  $\mathbf{g}_r = [g_{r,1}, g_{r,2}, \dots, g_{r,L_r}]^T \in \mathbb{C}^{L_r \times 1}$  are the vectors composed of the corresponding elements in  $\mathbf{g}$  according to  $\Lambda_s$  and  $\Lambda_r$ , and  $\mathbf{g}_s \in \mathbb{C}^{L_s \times 1}$  is denoted as the so-called DPGI in the following. Similarly, according to  $\Lambda_s$  and  $\Lambda_r$ , the sub-matrices composed of the corresponding column vectors in  $\mathbf{A}$  are expressed as  $\mathbf{A}_s = [\mathbf{a}_{s,1}, \mathbf{a}_{s,2}, \dots, \mathbf{a}_{s,L_s}] \in \mathbb{C}^{N_B \times L_s}$  and  $\mathbf{A}_r = [\mathbf{a}_{r,1}, \mathbf{a}_{r,2}, \dots, \mathbf{a}_{r,L_r}] \in \mathbb{C}^{N_B \times L_r}$ . Here we decompose the active beamformer  $\mathbf{f}_t \in \mathbb{C}^{N_B \times 1}$  into the product of two parts [25], [26]:

$$\mathbf{f}_t = \mathbf{V} \mathbf{g}_s^*, \quad (19)$$

where  $\mathbf{V} \in \mathbb{C}^{N_B \times L_s}$  is the active beamforming matrix to be optimized.

**Lemma 1:** By substituting (18) and (19) into the objective function  $\mathbb{E} \left[ |\mathbf{h}^H \mathbf{f}_t|^2 \right]$ , we have

$$\mathbb{E} \left[ |\mathbf{h}^H \mathbf{f}_t|^2 \right] = (4 - 2Q) \|\text{diag}(\mathbf{A}_s^H \mathbf{V})\|^2 + Q |\text{tr}(\mathbf{A}_s^H \mathbf{V})|^2 + Q \|\mathbf{A}_s^H \mathbf{V}\|_F^2 + Q \|\mathbf{A}_r^H \mathbf{V}\|_F^2, \quad (20)$$

where  $Q = \frac{L+L_{\text{RB}}+L_{\text{RU}}-3}{L-1}$  is defined for notational simplicity.

*Proof:* See Appendix A. ■

In the process of path selection, the index of the path with minimal contribution to  $R$  is removed from  $\{\Lambda_s\}$  sequentially, and the active and passive beamformers need to be optimized. Based on the above derivations, the initial optimization problem is expressed as

$$\mathcal{P}_1 : \max_{\{\Lambda_s, \mathbf{V}, \boldsymbol{\psi}\}} R, \text{ s.t. } |\Lambda_s| = L_s, \|\mathbf{V}\mathbf{g}_s^*\|^2 = 1, |\boldsymbol{\psi}| = \mathbf{1}_{N_{\text{R}} \times 1}, \quad (21)$$

where the second constraint in (21) is due to the power constraint  $\|\mathbf{f}_t\|^2 = \|\mathbf{V}\mathbf{g}_s^*\|^2 = 1$ . For a given  $\Lambda_s$ , the initial optimization problem  $\mathcal{P}_1$  can be simplified as

$$\mathcal{P}_2 : \max_{\{\mathbf{V}, \boldsymbol{\psi}\}} \mathbb{E} \left[ |\mathbf{h}^H \mathbf{f}_t|^2 \right], \text{ s.t. } \|\mathbf{V}\|_{\text{F}}^2 = 1, |\boldsymbol{\psi}| = \mathbf{1}_{N_{\text{R}} \times 1}, \quad (22)$$

where the first constraint in (22) is adopted instead of the second constraint in (21) because  $\mathbf{g}_s$  (DPGI) has not been acquired at BS during the process of path selection.<sup>4</sup> Due to the two types of constraints in (22)  $\mathbf{V}$  and  $\boldsymbol{\psi}$  cannot be optimized jointly, and thus we employ the alternating optimization of the active and passive beamformers.

### 2) Active Beamforming Design:

We first consider the design of active beamforming matrix  $\mathbf{V}$  with fixed  $\Lambda_s$  and  $\boldsymbol{\psi}$ , which can be given by

$$\mathcal{P}_3 : \max_{\{\mathbf{V}\}} \mathbb{E} \left[ |\mathbf{h}^H \mathbf{f}_t|^2 \right], \text{ s.t. } \|\mathbf{V}\|_{\text{F}}^2 = 1. \quad (23)$$

On the basis of (20), the objective function of (23) can be equivalently rewritten as

$$\mathbb{E} \left[ |\mathbf{h}^H \mathbf{f}_t|^2 \right] = \mathbf{v}^H \mathbf{J}_{\text{act}} \mathbf{v}, \quad (24)$$

where  $\mathbf{v} = \text{vec}(\mathbf{V}) \in \mathbb{C}^{N_{\text{B}}L_s \times 1}$  is the vectorization of active beamforming matrix  $\mathbf{V}$ , and  $\mathbf{J}_{\text{act}} \in \mathbb{C}^{N_{\text{B}}L_s \times N_{\text{B}}L_s}$  is

$$\begin{aligned} \mathbf{J}_{\text{act}} = & (4 - 2Q) \text{diag} (\mathbf{a}_{s,1} \mathbf{a}_{s,1}^H, \mathbf{a}_{s,2} \mathbf{a}_{s,2}^H, \dots, \mathbf{a}_{s,L_s} \mathbf{a}_{s,L_s}^H) + Q \text{vec}(\mathbf{A}_s) (\text{vec}(\mathbf{A}_s))^H \\ & + Q (\mathbf{I}_{L_s} \otimes \mathbf{A}_s^H)^H (\mathbf{I}_{L_s} \otimes \mathbf{A}_s^H) + Q (\mathbf{I}_{L_s} \otimes \mathbf{A}_r^H)^H (\mathbf{I}_{L_s} \otimes \mathbf{A}_r^H), \end{aligned} \quad (25)$$

<sup>4</sup>We note that this approximation scales the contributions to  $\mathbb{E} \left[ |\mathbf{h}^H \mathbf{f}_t|^2 \right]$  (the components related to each path in  $\mathbb{E} \left[ |\mathbf{h}^H \mathbf{f}_t|^2 \right]$  are separated and formulated in (46) as below) of all the remaining dominant paths with a same proportion  $\frac{\|\mathbf{V}\mathbf{g}_s^*\|^2}{\|\mathbf{V}\|_{\text{F}}^2}$ , so it will not result in performance degradation for the path selection.

where the following properties are used

$$\|\text{diag}(\mathbf{A}_s^H \mathbf{V})\|^2 = \mathbf{v}^H \text{diag}(\mathbf{a}_{s,1} \mathbf{a}_{s,1}^H, \mathbf{a}_{s,2} \mathbf{a}_{s,2}^H, \dots, \mathbf{a}_{s,L_s} \mathbf{a}_{s,L_s}^H) \mathbf{v}, \quad (26)$$

$$|\text{tr}(\mathbf{A}_s^H \mathbf{V})|^2 = \mathbf{v}^H \text{vec}(\mathbf{A}_s) (\text{vec}(\mathbf{A}_s))^H \mathbf{v}, \quad (27)$$

$$\|\mathbf{A}_s^H \mathbf{V}\|_F^2 = \mathbf{v}^H (\mathbf{I}_{L_s} \otimes \mathbf{A}_s^H)^H (\mathbf{I}_{L_s} \otimes \mathbf{A}_s^H) \mathbf{v}, \quad (28)$$

$$\|\mathbf{A}_r^H \mathbf{V}\|_F^2 = \mathbf{v}^H (\mathbf{I}_{L_s} \otimes \mathbf{A}_r^H)^H (\mathbf{I}_{L_s} \otimes \mathbf{A}_r^H) \mathbf{v}. \quad (29)$$

Therefore, based on the formulation of (24), the optimal solution  $\mathbf{V}^*$  of  $\mathcal{P}_3$  is given by [26]

$$\mathbf{V}^* = \frac{1}{\|\mathbf{u}_{\text{act},\text{max}}\|} \text{invec}(\mathbf{u}_{\text{act},\text{max}}) \in \mathbb{C}^{N_B \times L_s}, \quad (30)$$

where  $\mathbf{u}_{\text{act},\text{max}} \in \mathbb{C}^{N_B L_s \times 1}$  is the eigenvector corresponding to the largest eigenvalue of  $\mathbf{J}_{\text{act}}$ .

### 3) Passive Beamforming Design:

After the optimization of the active beamforming matrix  $\mathbf{V}$ . We design the passive beamforming vector  $\boldsymbol{\psi}$  with fixed  $\Lambda_s$  and  $\mathbf{V}$ . The optimization problem is formulated as

$$\mathcal{P}_4 : \max_{\{\boldsymbol{\psi}\}} \mathbb{E} \left[ |\mathbf{h}^H \mathbf{f}_t|^2 \right], \text{ s.t. } |\boldsymbol{\psi}| = \mathbf{1}_{N_R \times 1}. \quad (31)$$

According to (16) and (17), by defining  $\mathbf{B}_{s,l_s} \in \mathbb{C}^{N_B \times N_R}$  and  $\mathbf{B}_{r,l_r} \in \mathbb{C}^{N_B \times N_R}$  corresponding to the selected  $L_s$  dominant paths and the removed  $L_r$  paths, respectively, we have

$$\mathbf{a}_{s,l_s} = \mathbf{B}_{s,l_s} \boldsymbol{\psi}^* \in \mathbb{C}^{N_B \times 1} \text{ for } l_s = 1, 2, \dots, L_s, \quad (32)$$

$$\mathbf{a}_{r,l_r} = \mathbf{B}_{r,l_r} \boldsymbol{\psi}^* \in \mathbb{C}^{N_B \times 1} \text{ for } l_r = 1, 2, \dots, L_r. \quad (33)$$

Then, the objective function in (31) can be rewritten as

$$\mathbb{E} \left[ |\mathbf{h}^H \mathbf{f}_t|^2 \right] = \boldsymbol{\psi}^H \mathbf{J}_{\text{pass}} \boldsymbol{\psi}. \quad (34)$$

The intermediate variable  $\mathbf{J}_{\text{pass}} \in \mathbb{C}^{N_R \times N_R}$  is given by

$$\begin{aligned} \mathbf{J}_{\text{pass}} = & (4 - 2Q) \sum_{l_s=1}^{L_s} \mathbf{B}_{s,l_s}^T \mathbf{v}_{l_s}^* \mathbf{v}_{l_s}^T \mathbf{B}_{s,l_s}^* + Q \left( \sum_{l_s=1}^{L_s} \mathbf{B}_{s,l_s}^T \mathbf{v}_{l_s}^* \right) \left( \sum_{l_s=1}^{L_s} \mathbf{v}_{l_s}^T \mathbf{B}_{s,l_s}^* \right) \\ & + Q \left( \sum_{l_s=1}^{L_s} \mathbf{B}_{s,l_s}^T \boldsymbol{\Upsilon}_{s,l_s}^T \right) \left( \sum_{l_s=1}^{L_s} \boldsymbol{\Upsilon}_{s,l_s}^* \mathbf{B}_{s,l_s}^* \right) + Q \left( \sum_{l_r=1}^{L_r} \mathbf{B}_{r,l_r}^T \boldsymbol{\Upsilon}_{r,l_r}^T \right) \left( \sum_{l_r=1}^{L_r} \boldsymbol{\Upsilon}_{r,l_r}^* \mathbf{B}_{r,l_r}^* \right), \end{aligned} \quad (35)$$

where we define

$$\boldsymbol{\Upsilon}_s = \mathbf{I}_{L_s} \otimes \mathbf{V}^H = [\boldsymbol{\Upsilon}_{s,1}, \boldsymbol{\Upsilon}_{s,2}, \dots, \boldsymbol{\Upsilon}_{s,L_s}] \in \mathbb{C}^{L_s^2 \times N_B L_s} \text{ with } \boldsymbol{\Upsilon}_{s,l_s} \in \mathbb{C}^{L_s^2 \times N_B}, \quad (36)$$

$$\boldsymbol{\Upsilon}_r = \mathbf{I}_{L_r} \otimes \mathbf{V}^H = [\boldsymbol{\Upsilon}_{r,1}, \boldsymbol{\Upsilon}_{r,2}, \dots, \boldsymbol{\Upsilon}_{r,L_r}] \in \mathbb{C}^{L_s L_r \times N_B L_r} \text{ with } \boldsymbol{\Upsilon}_{r,l_r} \in \mathbb{C}^{L_s L_r \times N_B}. \quad (37)$$

In addition, the properties

$$\|\text{diag}(\mathbf{A}_s^H \mathbf{V})\|^2 = \boldsymbol{\psi}^H \left( \sum_{l_s=1}^{L_s} \mathbf{B}_{s,l_s}^T \mathbf{v}_{l_s}^* \mathbf{v}_{l_s}^T \mathbf{B}_{s,l_s}^* \right) \boldsymbol{\psi}, \quad (38)$$

$$|\text{tr}(\mathbf{A}_s^H \mathbf{V})|^2 = \boldsymbol{\psi}^H \left( \sum_{l_s=1}^{L_s} \mathbf{B}_{s,l_s}^T \mathbf{v}_{l_s}^* \right) \left( \sum_{l_s=1}^{L_s} \mathbf{v}_{l_s}^T \mathbf{B}_{s,l_s}^* \right) \boldsymbol{\psi}, \quad (39)$$

$$\|\mathbf{A}_s^H \mathbf{V}\|_F^2 = \boldsymbol{\psi}^H \left( \sum_{l_s=1}^{L_s} \mathbf{B}_{s,l_s}^T \boldsymbol{\Upsilon}_{s,l_s}^T \right) \left( \sum_{l_s=1}^{L_s} \boldsymbol{\Upsilon}_{s,l_s}^* \mathbf{B}_{s,l_s}^* \right) \boldsymbol{\psi}, \quad (40)$$

$$\|\mathbf{A}_r^H \mathbf{V}\|_F^2 = \boldsymbol{\psi}^H \left( \sum_{l_r=1}^{L_r} \mathbf{B}_{r,l_r}^T \boldsymbol{\Upsilon}_{r,l_r}^T \right) \left( \sum_{l_r=1}^{L_r} \boldsymbol{\Upsilon}_{r,l_r}^* \mathbf{B}_{r,l_r}^* \right) \boldsymbol{\psi} \quad (41)$$

are used here. Then,  $\mathcal{P}_4$  is equivalently re-expressed as

$$\mathcal{P}_4 : \min_{\{\boldsymbol{\psi}\}} f(\boldsymbol{\psi}), \quad \text{s.t. } |\boldsymbol{\psi}| = \mathbf{1}_{N_R \times 1}, \quad (42)$$

where the objective function to be minimized is defined as  $f(\boldsymbol{\psi}) = -\boldsymbol{\psi}^H \mathbf{J}_{\text{pass}} \boldsymbol{\psi}$  [38]. Considering the continuous and differentiable properties of  $f(\boldsymbol{\psi})$  as well as the non-convex constant modulus constraints imposed on  $\boldsymbol{\psi}$ , we employ the manifold optimization theory to solve  $\mathcal{P}_4$  (see [39], for details).

We begin with defining the complex circle manifold (called Riemannian manifold) formed by unit modulus constraints in (42) as  $\mathcal{M}_{cc}^{N_R} = \{\boldsymbol{\psi} : |\boldsymbol{\psi}| = \mathbf{1}_{N_R \times 1}\}$ . Then, the tangent space for any given point  $\boldsymbol{\psi}$  on  $\mathcal{M}_{cc}^{N_R}$  is expressed as  $T_{\boldsymbol{\psi}} \mathcal{M}_{cc}^{N_R} = \{\mathbf{z} : \Re\{\boldsymbol{\psi}^* \odot \mathbf{z}\} = \mathbf{0}_{N_R \times 1}\}$ . The classical conjugate gradient descent method can be used for the manifold optimization by projecting the gradient in the Euclidean space onto the Riemannian space [27], [39]. Thus, we can express the Riemannian gradient as  $\text{grad} f(\boldsymbol{\psi}) = \nabla f(\boldsymbol{\psi}) - \Re\{\nabla f(\boldsymbol{\psi}) \odot \boldsymbol{\psi}^*\} \odot \boldsymbol{\psi} \in \mathbb{C}^{N_R \times 1}$ , where  $\nabla f(\boldsymbol{\psi}) = -\mathbf{J}_{\text{pass}}^H \boldsymbol{\psi} \in \mathbb{C}^{N_R \times 1}$  denotes the Euclidean gradient and  $\mathbf{J}_{\text{pass}}$  is a Hermitian matrix. The conjugate direction  $\mathbf{d} \in \mathbb{C}^{N_R \times 1}$  on the Riemannian manifold is given by

$$\mathbf{d} = -\text{grad} f(\boldsymbol{\psi}) + \tau_1 \mathcal{T}(\bar{\mathbf{d}}), \quad (43)$$

where

$$\mathcal{T}(\bar{\mathbf{d}}) = \bar{\mathbf{d}} - \Re\{\bar{\mathbf{d}} \odot \boldsymbol{\psi}^*\} \odot \boldsymbol{\psi}. \quad (44)$$

$\bar{\mathbf{d}}$  denotes the previous conjugate direction, and  $\tau_1$  denotes the Polak-Ribiere parameter [39]. Finally, we map the updated point onto the manifold by a retraction operation (i.e. an operation to move along the conjugate direction  $\mathbf{d}$  while staying on the manifold) given by

$$\boldsymbol{\psi} \leftarrow \frac{\boldsymbol{\psi} + \tau_2 \mathbf{d}}{|\boldsymbol{\psi} + \tau_2 \mathbf{d}|}, \quad (45)$$

where the step size  $\tau_2$  can be found through Armijo backtracking line search [39]. The overall algorithm is summarized as Algorithm 1, and the convergence of the proposed algorithm is guaranteed according to Theorem 4.3.1 in [39].

---

**Algorithm 1:** Manifold Optimization for Solving  $\mathcal{P}_4$ .

---

**Input:**  $\mathbf{J}_{\text{pass}}$  and initial point  $\boldsymbol{\psi}$ .

- 1 Initialization: Index of iterations  $i \leftarrow 0$ ;  $\boldsymbol{\psi}^{(0)} = \boldsymbol{\psi}$ ;  $\mathbf{d}^{(0)} = -\text{grad } f(\boldsymbol{\psi}^{(0)})$
- 2 **repeat**
- 3     Compute the Armijo backtracking line search step size  $\tau_2$  ;
- 4     Update the passive beamformer as  $\boldsymbol{\psi}^{(i+1)}$  by (45) ;
- 5     Compute the Riemannian gradient at  $\boldsymbol{\psi}^{(i+1)}$ , the Polak-Ribiere parameter  $\tau_1$ , and the transpose from  $\boldsymbol{\psi}^{(i)}$  to  $\boldsymbol{\psi}^{(i+1)}$  ;
- 6     Update the conjugate direction as  $\mathbf{d}^{(i+1)}$  according to (43) ;
- 7      $i \leftarrow i + 1$  ;
- 8 **until**  $|f(\boldsymbol{\psi}^{(i+1)}) - f(\boldsymbol{\psi}^{(i)})|$  converges;

**Output:**  $\boldsymbol{\psi}^{(i+1)}$

---

4) *Proposed Path Selection Algorithm:*

After solving the alternating optimization of active and passive beamformers, we perform the path selection. In the proposed path selection strategy, to maximize the achievable downlink spectral efficiency  $R$ , the path with minimal contribution to  $R$  is removed sequentially. Specifically, according to (20) for  $l_s = 1, 2, \dots, L_s$ , the component related to the  $l_s$ -th path is separated from  $\mathbb{E} \left[ |\mathbf{h}^H \mathbf{f}_t|^2 \right]$  and defined as  $\zeta(l_s)$ , which is given by

$$\begin{aligned} \zeta(l_s) = & (4 - 2Q) \mathbf{v}_{l_s}^H \mathbf{a}_{s,l_s} \mathbf{a}_{s,l_s}^H \mathbf{v}_{l_s} + Q \left( \mathbf{v}_{l_s}^H \mathbf{a}_{s,l_s} \mathbf{a}_{s,l_s}^H \mathbf{v}_{l_s} + 2\Re \left[ \sum_{i \neq l_s}^{L_s} \mathbf{v}_{l_s}^H \mathbf{a}_{s,l_s} \mathbf{a}_{s,i}^H \mathbf{v}_i \right] \right) \\ & + Q \|\mathbf{A}_s^H \mathbf{v}_{l_s}\|^2 + Q \|\mathbf{A}_r^H \mathbf{v}_{l_s}\|^2. \end{aligned} \quad (46)$$

The overall path selection algorithm is summarized in Algorithm 2.

---

**Algorithm 2:** Proposed Path Selection Algorithm.

---

**Input:**  $\mathbf{B}_l \in \mathbb{C}^{N_B \times N_R}$  for  $l = 1, \dots, L$  in (17),  $L_{RB}$ , and  $L_{RU}$ .

- 1 Initialization:  $\Lambda_s = \{1, 2, \dots, L\}$ ;  $\boldsymbol{\psi} = \mathbf{1}_{N_R \times 1}$
- 2 **repeat**
- 3     **repeat**
- 4         Compute  $\mathbf{A}$ ,  $\mathbf{A}_s$ , and  $\mathbf{A}_r$  according to  $\Lambda_s$ ,  $\boldsymbol{\psi}$ , and  $\mathbf{B}_l$  for  $l = 1, \dots, L$  (see (15)-(17)) ;
- 5         Optimize  $\mathbf{V}$  with fixed  $\boldsymbol{\psi}$  by solving  $\mathcal{P}_3$  ;
- 6         Optimize  $\boldsymbol{\psi}$  with fixed  $\mathbf{V}$  by solving  $\mathcal{P}_4$  according to Algorithm 1 ;
- 7     **until** the objective value of  $\mathbb{E} \left[ |\mathbf{h}^H \mathbf{f}_t|^2 \right]$  in  $\mathcal{P}_2$  converges;
- 8     Find the path index denoted as  $\hat{l}_s$  with minimal  $\zeta(\hat{l}_s)$  by (46) for  $\hat{l}_s \in \{1, 2, \dots, L_s\}$  ;
- 9     Update  $\{\Lambda_s\}$  by removing its  $\hat{l}_s$ -th element ;
- 10      $L_s \leftarrow L_s - 1$  ;
- 11 **until**  $L_s$  reaches the pre-given number of dominant paths;

**Output:**  $\Lambda_s$

---

### B. DPGI Estimation and Feedback

Once the path selection is finished, we perform the acquisition of  $\mathbf{g}_s \in \mathbb{C}^{L_s \times 1}$  (downlink DPGI) at BS. For  $t = 1, 2, \dots, L_s$ , pilot symbol denoted as  $s(t)$  is sent at BS within  $L_s$  time slots. Then, based on (10), the signal received at UE in the  $t$ -th time slot is given by

$$y(t) = \sqrt{\frac{P_e N_B N_R^2}{L}} \boldsymbol{\beta}^T \mathbf{A}_{RU}^H \text{diag}(\boldsymbol{\psi}(t)) \mathbf{A}_{RB} \text{diag}(\boldsymbol{\alpha}) \mathbf{A}_B^H \mathbf{f}_e(t) s(t) + n(t), \quad (47)$$

where  $P_e$  is the transmitting power for DPGI estimation,  $n(t) \sim \mathcal{CN}(0, \sigma_n^2)$  is the complex Gaussian noise with noise power  $\sigma_n^2$ . In addition,  $\mathbf{f}_e(t) \in \mathbb{C}^{N_B \times 1}$  satisfying  $\|\mathbf{f}_e(t)\|^2 = 1$  represents the active beamforming vector for DPGI estimation (different from the  $\mathbf{f}_t$  defined in (19) for data transmission), and  $\boldsymbol{\psi}(t)$  denotes the passive beamforming vector in the  $t$ -th time slot for DPGI estimation satisfying  $|\boldsymbol{\psi}(t)| = \mathbf{1}_{N_R \times 1}$ . The performance of DPGI estimation can be improved by jointly designing the active and passive beamformers. By assuming  $s(t) = 1$ , for  $t = 1, 2, \dots, L_s$ ,

the received signal  $y(t)$  in (47) is re-expressed as

$$y(t) = \sqrt{\frac{P_e N_B N_R^2}{L}} \boldsymbol{\psi}^T(t) \tilde{\mathbf{A}}_R \text{diag}(\mathbf{g}) \tilde{\mathbf{A}}_B^H \mathbf{f}_e(t) + n(t) \quad (48)$$

$$= \sqrt{\frac{P_e N_B N_R^2}{L}} \left( \left( \mathbf{f}_e^T(t) \tilde{\mathbf{A}}_B^* \right) \odot \left( \boldsymbol{\psi}^T(t) \tilde{\mathbf{A}}_R \right) \right) \mathbf{g} + n(t) \quad (49)$$

$$= \boldsymbol{\kappa}^T(t) \mathbf{g} + n(t) \quad (50)$$

$$= \underbrace{\kappa_{\lambda_{s,t}}(t) g_{\lambda_{s,t}}}_{\text{To be maximized}} + \underbrace{\left( \sum_{l \neq \lambda_{s,t}}^L \kappa_l(t) g_l + n(t) \right)}_{\text{Equivalent noise}}, \quad (51)$$

where (48) is obtained by defining

$$\tilde{\mathbf{A}}_B = [\tilde{\mathbf{a}}_{B,1}, \tilde{\mathbf{a}}_{B,2}, \dots, \tilde{\mathbf{a}}_{B,L}] \in \mathbb{C}^{N_B \times L} \text{ with } \tilde{\mathbf{a}}_{B,l} = \mathbf{a}_{B,p} \in \mathbb{C}^{N_B \times 1}, \quad (52)$$

$$\tilde{\mathbf{A}}_R = [\tilde{\mathbf{a}}_{R,1}, \tilde{\mathbf{a}}_{R,2}, \dots, \tilde{\mathbf{a}}_{R,L}] \in \mathbb{C}^{N_R \times L} \text{ with } \tilde{\mathbf{a}}_{R,l} = \text{diag}(\mathbf{a}_{RU,q}^*) \mathbf{a}_{RB,p} \in \mathbb{C}^{N_R \times 1} \quad (53)$$

for the path index  $l = (q-1)L_{RB} + p$ ,  $p = 1, 2, \dots, L_{RB}$  and  $q = 1, 2, \dots, L_{RU}$ . Besides, (49) follows from the property of Hadamard product, and  $\boldsymbol{\kappa}(t)$  is defined as

$$\boldsymbol{\kappa}(t) = [\kappa_1(t), \kappa_2(t), \dots, \kappa_L(t)]^T = \sqrt{\frac{P_e N_B N_R^2}{L}} \left( \left( \mathbf{f}_e^T(t) \tilde{\mathbf{A}}_B^* \right) \odot \left( \boldsymbol{\psi}^T(t) \tilde{\mathbf{A}}_R \right) \right)^T \in \mathbb{C}^{L \times 1} \quad (54)$$

in (50) to simplify the expression. The strategy of DPGI estimation can be explained via (51). Specifically, for the selected  $L_s$  dominant paths, the corresponding active and passive beamforming vectors are jointly optimized in each time slot  $t = 1, 2, \dots, L_s$  to maximize  $\kappa_{\lambda_{s,t}}(t)$ , where  $\lambda_{s,t}$  denotes the  $t$ -th element in set  $\Lambda_s = \{\lambda_{s,1}, \lambda_{s,2}, \dots, \lambda_{s,L_s}\}$ . Then, the component corresponding to the  $t$ -th dominant path in (51) denoted as  $\kappa_{\lambda_{s,t}}(t) g_{\lambda_{s,t}}$  is maximized, and the rest components are considered as the equivalent noise.

Based on (49), the maximization of  $\kappa_{\lambda_{s,t}}(t)$  is equivalent to the maximization of the  $\lambda_{s,t}$ -th element in row vector  $\mathbf{f}_e^T(t) \tilde{\mathbf{A}}_B^* \in \mathbb{C}^{1 \times L}$  and the maximization of the  $\lambda_{s,t}$ -th element in row vector  $\boldsymbol{\psi}^T(t) \tilde{\mathbf{A}}_R \in \mathbb{C}^{1 \times L}$ . Therefore, the optimal solutions of jointly designed active beamformer  $\mathbf{f}_e(t)$  and passive beamformer  $\boldsymbol{\psi}(t)$  are given, respectively, by

$$\mathbf{f}_e(t) = \frac{\tilde{\mathbf{a}}_{B,\lambda_{s,t}}}{\|\tilde{\mathbf{a}}_{B,\lambda_{s,t}}\|} = \tilde{\mathbf{a}}_{B,\lambda_{s,t}}, \quad (55)$$

$$\boldsymbol{\psi}(t) = \frac{\tilde{\mathbf{a}}_{R,\lambda_{s,t}}^*}{|\tilde{\mathbf{a}}_{R,\lambda_{s,t}}^*|} = N_R \tilde{\mathbf{a}}_{R,\lambda_{s,t}}^*, \quad (56)$$



where we have  $\|\tilde{\mathbf{a}}_{\text{B},\lambda_{\text{s}},t}\| = 1$  and  $|\tilde{\mathbf{a}}_{\text{R},\lambda_{\text{s}},t}^*| = \frac{1}{N_{\text{R}}}\mathbf{1}_{N_{\text{R}} \times 1}$  according to their definitions. The power constraint and the constant modulus constraint are satisfied in (55) and (56), respectively. By substituting (55) and (56) into (54), we obtain

$$\kappa_{\lambda_{\text{s}},t}(t) = \sqrt{\frac{P_{\text{e}}N_{\text{B}}N_{\text{R}}^2}{L}}\mathbf{f}_{\text{e}}^{\text{T}}(t)\tilde{\mathbf{a}}_{\text{B},\lambda_{\text{s}},t}^*\boldsymbol{\psi}^{\text{T}}(t)\tilde{\mathbf{a}}_{\text{R},\lambda_{\text{s}},t} = \sqrt{\frac{P_{\text{e}}N_{\text{B}}N_{\text{R}}^2}{L}}. \quad (57)$$

We further have  $\mathbf{y} = [y(1), y(2), \dots, y(L_{\text{s}})]^{\text{T}} \in \mathbb{C}^{L_{\text{s}} \times 1}$  by concatenating  $L_{\text{s}}$  successive receiving signals. According to (51) and (57), the estimate of downlink DPGI at the UE is given by

$$\hat{\mathbf{g}}_{\text{s}} = \sqrt{\frac{L}{P_{\text{e}}N_{\text{B}}N_{\text{R}}^2}}\mathbf{y} \in \mathbb{C}^{L_{\text{s}} \times 1}. \quad (58)$$

Then, the RVQ codebook is adopted i.e.,  $\mathbf{C}_{\text{RVQ}} = [\mathbf{c}_1, \mathbf{c}_2, \dots, \mathbf{c}_{2^B}] \in \mathbb{C}^{L_{\text{s}} \times 2^B}$  with  $B$  bits for the uplink feedback of  $\hat{\mathbf{g}}_{\text{s}} \in \mathbb{C}^{L_{\text{s}} \times 1}$ . By normalizing the estimated DPGI as  $\tilde{\mathbf{g}}_{\text{s}} = \frac{\hat{\mathbf{g}}_{\text{s}}}{\|\hat{\mathbf{g}}_{\text{s}}\|} \in \mathbb{C}^{L_{\text{s}} \times 1}$  and choosing a corresponding feedback codeword  $\hat{i}$  according to (13), the quantized downlink DPGI acquired at BS is expressed as

$$\tilde{\mathbf{g}}_{\text{s}} = \|\hat{\mathbf{g}}_{\text{s}}\| \mathbf{c}_{\hat{i}}. \quad (59)$$

### C. Beamformers Update

Though the active beamforming matrix  $\mathbf{V}$  and passive beamforming vector  $\boldsymbol{\psi}$  for downlink data transmission are designed during path selection, it should be noted that the expression of  $\mathbb{E} \left[ |\mathbf{h}^{\text{H}}\mathbf{f}_{\text{t}}|^2 \right]$  in (20) is obtained based on the statistical information of  $\mathbf{g} \in \mathbb{C}^{L \times 1}$ , and the first constraint in (22) is approximated from the original power constraint in (21) for path selection. In this subsection, to further improve the spectral efficiency, we update the passive beamformer  $\boldsymbol{\psi}$  and the active beamformer  $\mathbf{f}_{\text{t}}$  by exploiting the quantized DPGI  $\tilde{\mathbf{g}}_{\text{s}}$ .<sup>5</sup>

#### 1) Problem Formulation:

After performing the proposed path selection algorithm together with DPGI estimation and feedback scheme, the index set of selected dominant paths  $\{\Lambda_{\text{s}}\}$  and the quantized DPGI  $\tilde{\mathbf{g}}_{\text{s}} \in \mathbb{C}^{L_{\text{s}} \times 1}$  are acquired at BS. Then, we further update the optimization problem based on  $\mathcal{P}_1$  as

$$\mathcal{P}_5 : \max_{\{\mathbf{f}_{\text{t}}, \boldsymbol{\psi}\}} \mathbb{E} \left[ |\mathbf{h}^{\text{H}}\mathbf{f}_{\text{t}}|^2 \right], \text{ s.t. } \|\mathbf{f}_{\text{t}}\|^2 = 1, |\boldsymbol{\psi}| = \mathbf{1}_{N_{\text{R}} \times 1}, \quad (60)$$

and alternating optimization is carried out between the update of  $\mathbf{f}_{\text{t}}$  and  $\boldsymbol{\psi}$  as below.

<sup>5</sup>Since the quantized downlink DPGI can be used for active and passive beamformers update, here we can adopt the direct optimization of  $\mathbf{f}_{\text{t}}$  instead of the indirect optimization of  $\mathbf{f}_{\text{t}}$  by solving  $\mathbf{V}$  according to  $\mathbf{f}_{\text{t}} = \mathbf{V}\mathbf{g}_{\text{s}}^*$  as defined in (19).

2) *Active Beamformer Update:*

On the basis of  $\mathcal{P}_5$ , the optimization of  $\mathbf{f}_t$  with fixed  $\boldsymbol{\psi}$  is formulated as

$$\mathcal{P}_6 : \max_{\{\mathbf{f}_t\}} \mathbb{E} \left[ |\mathbf{h}^H \mathbf{f}_t|^2 \right], \text{ s.t. } \|\mathbf{f}_t\|^2 = 1. \quad (61)$$

**Lemma 2:** We can further re-express  $\mathbb{E} \left[ |\mathbf{h}^H \mathbf{f}_t|^2 \right]$  in (61) as

$$\mathbb{E} \left[ |\mathbf{h}^H \mathbf{f}_t|^2 \right] = \|\mathbf{A}_r^H \mathbf{f}_t\|^2 + |\mathbf{g}_s^T \mathbf{A}_s^H \mathbf{f}_t|^2, \quad (62)$$

where  $\mathbf{g}_s$  is kept because BS has obtained its quantized estimate  $\tilde{\mathbf{g}}_s$ , and  $\mathbf{g}_r$  is removed in the final expression of expectation by using the statistical information of  $\mathbf{g}_r$ , which makes (62) different from (20) obtained in Lemma 1.

*Proof:* See Appendix B. ■

The objective function in (62) is further expressed as

$$\mathbb{E} \left[ |\mathbf{h}^H \mathbf{f}_t|^2 \right] = \mathbf{f}_t^H \tilde{\mathbf{J}}_{\text{act}} \mathbf{f}_t, \quad (63)$$

where  $\tilde{\mathbf{J}}_{\text{act}}$  is expressed as

$$\tilde{\mathbf{J}}_{\text{act}} = \mathbf{A}_r \mathbf{A}_r^H + \mathbf{A}_s \mathbf{g}_s^* \mathbf{g}_s^T \mathbf{A}_s^H \in \mathbb{C}^{N_B \times N_B}. \quad (64)$$

Then, we obtain the optimal solution  $\mathbf{f}_t^*$  of  $\mathcal{P}_6$  as

$$\mathbf{f}_t^* = \frac{\tilde{\mathbf{u}}_{\text{act}, \max}}{\|\tilde{\mathbf{u}}_{\text{act}, \max}\|} \in \mathbb{C}^{N_B \times 1}, \quad (65)$$

where  $\tilde{\mathbf{u}}_{\text{act}, \max} \in \mathbb{C}^{N_B \times L_s}$  denotes the eigenvector corresponding to the largest eigenvalue of  $\tilde{\mathbf{J}}_{\text{act}}$ .

3) *Passive Beamformer Update:*

On the basis of  $\mathcal{P}_5$ , the optimization of  $\boldsymbol{\psi}$  with fixed  $\mathbf{f}_t$  can be formulated as

$$\mathcal{P}_7 : \min_{\{\boldsymbol{\psi}\}} \tilde{f}(\boldsymbol{\psi}), \text{ s.t. } |\boldsymbol{\psi}| = \mathbf{1}_{N_R \times 1}, \quad (66)$$

where  $\tilde{f}(\boldsymbol{\psi}) = -\mathbb{E} \left[ |\mathbf{h}^H \mathbf{f}_t|^2 \right]$ . Furthermore, based on (62), we have  $\tilde{f}(\boldsymbol{\psi}) = -\boldsymbol{\psi}^H \tilde{\mathbf{J}}_{\text{pass}} \boldsymbol{\psi}$ , where

$$\tilde{\mathbf{J}}_{\text{pass}} = \left( \sum_{l_r=1}^{L_r} \mathbf{B}_{r,l_r}^T \boldsymbol{\Gamma}_{r,l_r} \right) \left( \sum_{l_r=1}^{L_r} \boldsymbol{\Gamma}_{r,l_r}^* \mathbf{B}_{r,l_r}^* \right) + \left( \sum_{l_s=1}^{L_s} \mathbf{B}_{s,l_s}^T \boldsymbol{\gamma}_{s,l_s} \right) \left( \sum_{l_s=1}^{L_s} \boldsymbol{\gamma}_{s,l_s}^T \mathbf{B}_{s,l_s}^* \right) \in \mathbb{C}^{N_R \times N_R}. \quad (67)$$

The intermediate variables  $\boldsymbol{\Gamma}_r$  and  $\boldsymbol{\gamma}_s$  are defined as

$$\boldsymbol{\Gamma}_r = \mathbf{I}_{L_r} \otimes \mathbf{f}_t^H = [\boldsymbol{\Gamma}_{r,1}, \boldsymbol{\Gamma}_{r,2}, \dots, \boldsymbol{\Gamma}_{r,L_r}] \in \mathbb{C}^{L_r \times N_B L_r} \text{ with } \boldsymbol{\Gamma}_{r,l_r} \in \mathbb{C}^{L_r \times N_B}, \quad (68)$$

$$\boldsymbol{\gamma}_s = \mathbf{g}_s \otimes \mathbf{f}_t = [\boldsymbol{\gamma}_{s,1}^T, \boldsymbol{\gamma}_{s,2}^T, \dots, \boldsymbol{\gamma}_{s,L_s}^T]^T \in \mathbb{C}^{N_B L_s \times 1} \text{ with } \boldsymbol{\gamma}_{s,l_s} \in \mathbb{C}^{N_B \times 1} \quad (69)$$

for  $l_r = 1, 2, \dots, L_r$  and  $l_s = 1, 2, \dots, L_s$ . Besides, the properties

$$\|\mathbf{A}_r^H \mathbf{f}_t\|^2 = \boldsymbol{\psi}^H \left( \sum_{l_r=1}^{L_r} \mathbf{B}_{r,l_r}^T \boldsymbol{\Gamma}_{r,l_r}^T \right) \left( \sum_{l_r=1}^{L_r} \boldsymbol{\Gamma}_{r,l_r}^* \mathbf{B}_{r,l_r}^* \right) \boldsymbol{\psi}, \quad (70)$$

$$|\mathbf{g}_s^T \mathbf{A}_s^H \mathbf{f}_t|^2 = \boldsymbol{\psi}^H \left( \sum_{l_s=1}^{L_s} \mathbf{B}_{s,l_s}^T \gamma_{s,l_s}^* \right) \left( \sum_{l_s=1}^{L_s} \gamma_{s,l_s}^T \mathbf{B}_{s,l_s}^* \right) \boldsymbol{\psi} \quad (71)$$

are used here. By replacing  $f(\boldsymbol{\psi})$  in (42) with  $\tilde{f}(\boldsymbol{\psi})$  in (66), the Riemannian manifold optimization summarized in Algorithm 1 can be used to solve  $\mathcal{P}_7$ , using which the passive beamformer  $\boldsymbol{\psi}$  is updated [27], [39].

#### 4) Proposed Alternating Optimization Algorithm:

The overall alternating optimization algorithm is summarized in Algorithm 3.

---

**Algorithm 3:** Proposed Alternating Optimization for Solving  $\mathcal{P}_5$ .

---

**Input:**  $\mathbf{B}_l \in \mathbb{C}^{N_B \times N_R}$  for  $l = 1, \dots, L$  in (17),  $\{\Lambda_s\}$ , and  $\tilde{\mathbf{g}}_s$ .

1 Initialization:  $\boldsymbol{\psi} = \mathbf{1}_{N_R \times 1}$

2 **repeat**

3     Compute  $\mathbf{A}$ ,  $\mathbf{A}_s$ , and  $\mathbf{A}_r$  according to  $\Lambda_s$ ,  $\boldsymbol{\psi}$ , and  $\mathbf{B}_l$  for  $l = 1, \dots, L$  (see (15)-(17)) ;

4     Update  $\mathbf{f}_t$  with fixed  $\boldsymbol{\psi}$  by solving  $\mathcal{P}_6$  ;

5     Update  $\boldsymbol{\psi}$  with fixed  $\mathbf{f}_t$  by solving  $\mathcal{P}_7$  according to Algorithm 1 ;

6 **until** the objective value of  $\mathbb{E} \left[ |\mathbf{h}^H \mathbf{f}_t|^2 \right]$  in  $\mathcal{P}_5$  converges;

**Output:** The updated active beamformer  $\mathbf{f}_t$  and passive beamformer  $\boldsymbol{\psi}$

---

## IV. SIMULATION RESULTS

In this section, we evaluate the performance of proposed algorithms. In our simulations, we consider a FDD RIS-assisted mmWave wireless communication system, where BS is equipped with  $N_B = N_{B,v} \times N_{B,h} = 4 \times 4$  antennas and UE is equipped with single antenna. Besides, an RIS is equipped with  $N_R = N_{R,v} \times N_{R,h} = 16 \times 16$  reflecting elements. We adopt the channel model and signal model in (10) and (11) with  $L_{RB} = 2$ ,  $L_{RU} = 3$ , and  $\alpha_n = 1$ , where the AoAs/AoDs are assumed to be uniformly distributed in  $(0, \pi]$ . In this paper, we define two types of signal-to-noise ratio (SNR) [27]. The pilot-to-noise ratio (PNR) is defined as  $10 \log_{10} (P_e / \sigma_n^2)$ , where  $P_e$  denotes the transmitting power for DPGI estimation in (47). Similarly, the data-to-noise ratio (DNR) is defined as  $10 \log_{10} (P_t / \sigma_n^2)$ , where  $P_t$  represents the transmitting power for data transmission in (11). All results are obtained over 1,000 randomly generated realizations to avoid overfitting to special scenarios.

### A. Performance of DPGI Estimation and Feedback

In this subsection, the proposed DPGI estimation and feedback scheme are compared with several estimators based on existing schemes. To the best of our knowledge, no existing literature provides any scheme for the estimation of DPGI  $\mathbf{g}_s \in \mathbb{C}^{L_s \times 1}$  (rather than the whole PGI  $\mathbf{g} \in \mathbb{C}^{L \times 1}$ ) based on the known PAI in RIS-assisted systems. Therefore, in order to form effective comparisons, we not only provide simulation results of the proposed scheme with  $L_s < L$ , but also consider the scenario of  $L_s = L$ , where all the cascaded paths are used for the dominant paths, and simulation results of extending our proposed scheme to estimate the whole PGI  $\mathbf{g} \in \mathbb{C}^{L \times 1}$  are provided. The Oracle LS estimator in [21] and the MMSE estimator in [35] are used for the estimation of PGI  $\mathbf{g} \in \mathbb{C}^{L \times 1}$  to form effective comparisons with the proposed DPGI estimation and feedback scheme when  $L_s = L = 6$ .

Here we provide the processes of Oracle LS estimator and MMSE estimator as follows. Based on the signal model in (48), downlink pilot signals are sent from BS within  $T$  successive time slots, where  $s(t) = 1$  for  $t = 1, 2, \dots, T$ . The signal received at UE is given by  $y(t) = \mathbf{d}^T(t)\mathbf{g} + n(t)$ , where we define

$$\mathbf{d}(t) = [d_1(t), d_2(t), \dots, d_L(t)]^T = \sqrt{\frac{P_e N_B N_R^2}{L}} \left( \left( \mathbf{f}_e^T(t) \tilde{\mathbf{A}}_B^* \right) \odot \left( \boldsymbol{\psi}^T(t) \tilde{\mathbf{A}}_R \right) \right)^T \in \mathbb{C}^{L \times 1}. \quad (72)$$

Different from the  $\boldsymbol{\kappa}(t)$  defined in (54), here we additionally define  $\mathbf{d}(t)$  because the active beamforming vector  $\mathbf{f}_e(t)$  and the passive beamforming vector  $\boldsymbol{\psi}(t)$  used in Oracle LS estimator and MMSE estimator are randomly generated. By concatenating the signals within  $T$  time slots, we have  $\mathbf{y} = \mathbf{D}^T \mathbf{g} + \mathbf{n}$ , where  $\mathbf{y} = [y(1), y(2), \dots, y(T)]^T \in \mathbb{C}^{T \times 1}$ ,  $\mathbf{D} = [\mathbf{d}(1), \mathbf{d}(2), \dots, \mathbf{d}(T)] \in \mathbb{C}^{L \times T}$ , and  $\mathbf{n} = [n(1), n(2), \dots, n(T)]^T \in \mathbb{C}^{T \times 1}$ . We note that BS estimates PAI through the uplink pilot signals (which has been discussed in Subsection II-B), but the matrices  $\tilde{\mathbf{A}}_B$  and  $\tilde{\mathbf{A}}_R$  defined in (52) containing PAI are unavailable at UE. Therefore, the matrix  $\mathbf{D}$  is also not available at UE according to (72). For this reason, UE cannot estimate the PGI directly, and hence the received signals  $\mathbf{y}$  needs to be fed back in uplink and the PGI estimation is performed at BS, where  $T$  (the number of pilot signals) must be greater than or equal to  $L$  (the length of PGI) to avoid under-determination estimations [35]. Then, the RVQ codebook defined in (13) is used for the uplink feedback of  $\mathbf{y}$ , and Oracle LS estimator and MMSE estimator are performed at BS by exploiting the quantized vector of received signals (denoted as  $\tilde{\mathbf{y}}$ ), which are given by  $\hat{\mathbf{g}}_{LS} = (\mathbf{D}^* \mathbf{D}^T)^{-1} \mathbf{D}^* \tilde{\mathbf{y}} \in \mathbb{C}^{L \times 1}$  and  $\hat{\mathbf{g}}_{MMSE} = \mathbf{D}^* (\mathbf{D}^T \mathbf{D}^* + \sigma_n^2 \mathbf{I}_T)^{-1} \tilde{\mathbf{y}} \in \mathbb{C}^{L \times 1}$  [21], [35], [40].

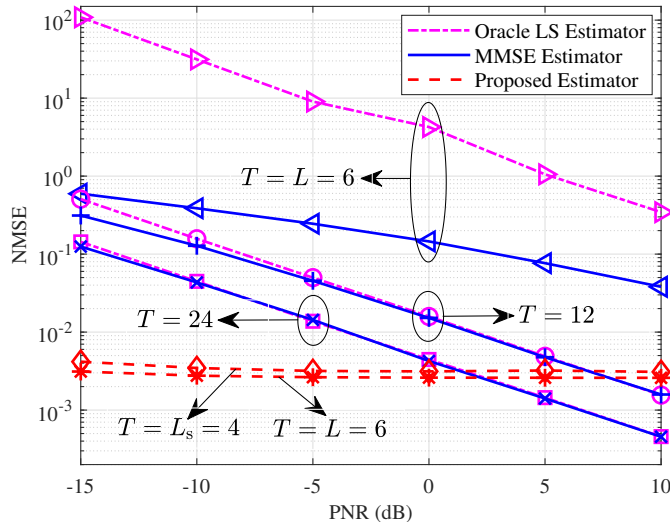


Fig. 2. NMSE performance against PNR when  $N_B = N_{B,v} \times N_{B,h} = 4 \times 4$ ,  $N_R = N_{R,v} \times N_{R,h} = 16 \times 16$ ,  $L = L_{RB} \times L_{RU} = 2 \times 3$ .

To evaluate the accuracy of DPGI/PGI estimation, the normalized mean square errors (NMSEs) against PNR are shown in Fig. 2. For the scenario of  $L_s < L$ , NMSE is expressed as  $10 \log_{10} (\mathbb{E} [\|\tilde{\mathbf{g}}_s - \mathbf{g}_s\|^2 / \|\mathbf{g}_s\|^2])$ , where  $\tilde{\mathbf{g}}_s \in \mathbb{C}^{L_s \times 1}$  denotes the quantized downlink DPGI acquired at BS in (59). For the scenario of  $L_s = L$ , NMSE is given by  $10 \log_{10} (\mathbb{E} [\|\tilde{\mathbf{g}}_s - \mathbf{g}\|^2 / \|\mathbf{g}\|^2])$ . In addition, the NMSEs of Oracle LS estimator and MMSE estimator are respectively expressed as  $10 \log_{10} (\mathbb{E} [\|\hat{\mathbf{g}}_{LS} - \mathbf{g}\|^2 / \|\mathbf{g}\|^2])$  and  $10 \log_{10} (\mathbb{E} [\|\hat{\mathbf{g}}_{MMSE} - \mathbf{g}\|^2 / \|\mathbf{g}\|^2])$  [28].<sup>6</sup>

It can be observed from Fig. 2 that the proposed DPGI/PGI scheme performs significantly better than the conventional schemes at relatively low PNR (-15dB  $\sim$  0dB). Compared with the proposed scheme which requires only  $T = L_s$  pilot signals, much more pilot signals are required for both Oracle LS estimator and MMSE estimator to achieve a comparable accuracy of estimation. Besides, the equivalent noise of proposed scheme in (51) is composed of two parts, which are the channel noise  $n(t)$  and interference from other  $(L - 1)$  paths denoted as  $\sum_{l \neq \lambda_{s,t}}^L \kappa_l(t) g_l$ . The estimation accuracy of proposed scheme is mainly affected by the channel

<sup>6</sup>Different from our proposed estimator, UE side cannot perform the PGI/DPGI estimation for Oracle LS estimator and MMSE estimator because PAI is not available at UE, which means that the gains of different paths cannot be obtained and separated at UE. Therefore, received signal vector  $\mathbf{y} \in \mathbb{C}^{T \times 1}$  has to be fed back in uplink and the whole PGI (i.e. gains of all  $L$  cascaded paths) will be estimated at BS.

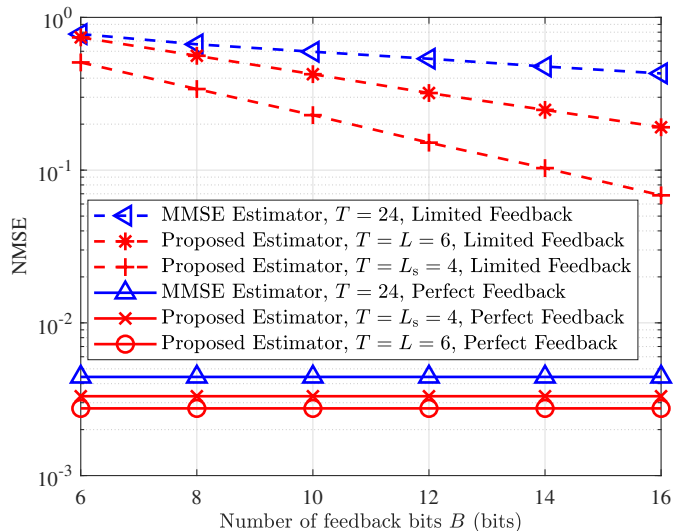


Fig. 3. NMSE performance against number of feedback bits  $B$  when  $N_B = N_{B,v} \times N_{B,h} = 4 \times 4$ ,  $N_R = N_{R,v} \times N_{R,h} = 16 \times 16$ ,  $L = L_{RB} \times L_{RU} = 2 \times 3$ , PNR = 0 dB.

noise at first, so NMSE decreases slowly with PNR in the interval -15dB to -5dB. Then, the interference of other paths dominates the equivalent noise around when  $\text{PNR} > -5\text{dB}$ , so the NMSE curves of proposed estimator tend to be stable. In addition, the NMSE performance of MMSE estimator is better than that of Oracle LS estimator, so we will only adopt MMSE estimator (with  $T = 24$ ) in the following simulations.

Fig. 3 shows the NMSE performance against the number of feedback bits  $B$  when  $\text{PNR} = 0$  dB. The solid lines refer to the case using perfect feedback ( $B \rightarrow \infty$ ) and dashed lines refer to the case with limited feedback. In terms of the NMSE performance, the proposed estimator outperforms MMSE estimator with limited  $B$  for two main reasons detailed below. On the one hand, the minimal achievable NMSE of proposed estimator (corresponding to solid lines when  $B \rightarrow \infty$ ) is lower than that of MMSE estimator. On the other hand, the pilot length of proposed estimator (i.e.  $T$ , equal to the length of feedback vector) is smaller, so the inevitable quantization error caused by RVQ feedback of proposed estimator is smaller than that of MMSE estimator with fixed  $B$ , which also explains why the achievable NMSE with  $T = L_s = 4$  is lower than the achievable NMSE with  $T = L = 6$  for limited feedback scenario.

### B. Performance of Path Selection and Beamforming

In this subsection, we compare the proposed path selection and beamforming scheme with conventional beamforming schemes. To form an effective comparison, the alternating optimization proposed in [7] is also simulated, which can be used for the design of active beamformer  $\mathbf{f}_t$  and passive beamformer  $\boldsymbol{\psi}$ . Specifically, by defining

$$\mathbf{H} = \sqrt{\frac{N_B N_R^2}{L}} \tilde{\mathbf{A}}_R \text{diag}(\mathbf{g}) \tilde{\mathbf{A}}_B^H \in \mathbb{C}^{N_R \times N_B} \quad (73)$$

according to (48), the cascaded channel is re-expressed as  $\mathbf{h}^H = \boldsymbol{\psi}^T \mathbf{H} \in \mathbb{C}^{1 \times N_B}$ , and the objective function  $\mathbb{E} \left[ |\mathbf{h}^H \mathbf{f}_t|^2 \right]$  is transformed into  $\mathbb{E} \left[ |\boldsymbol{\psi}^T \mathbf{H} \mathbf{f}_t|^2 \right]$ . Then, active beamformer  $\mathbf{f}_t$  and passive beamformer  $\boldsymbol{\psi}$  are alternatively optimized by  $\mathbf{f}_t = \frac{\mathbf{H}^H \boldsymbol{\psi}^*}{\|\mathbf{H}^H \boldsymbol{\psi}^*\|} \in \mathbb{C}^{N_B \times 1}$  and  $\boldsymbol{\psi} = \frac{\mathbf{H}^* \mathbf{f}_t^*}{|\mathbf{H} \mathbf{f}_t|} \in \mathbb{C}^{N_R \times 1}$  until  $|\boldsymbol{\psi}^T \mathbf{H} \mathbf{f}_t|^2$  converges [7]. For the case where the whole PGI (i.e.  $\mathbf{g} \in \mathbb{C}^{L \times 1}$ ) can be obtained, the quantized estimate of  $\mathbf{g} \in \mathbb{C}^{L \times 1}$  can be brought into (73) for subsequent alternating optimizations. In addition, for the case of  $T = L_s < L$ , a scheme named ‘Beamforming in [7] with Partial Random PGI’ is also provided to form an effective comparison with our proposed DPGI-based design of active beamformer and passive beamformer. Specifically, for the PGI (i.e.  $\mathbf{g} \in \mathbb{C}^{L \times 1}$ ) brought into (73), we assign the elements corresponding to selected dominant paths in  $\mathbf{g} \in \mathbb{C}^{L \times 1}$  to the value of quantized downlink DPGI  $\tilde{\mathbf{g}}_s \in \mathbb{C}^{L_s \times 1}$  in (59), and the remaining elements in  $\mathbf{g} \in \mathbb{C}^{L \times 1}$  with dimension of  $L_r \times 1$  are assigned to random values. Then, the alternating iteration proposed in [7] is adopted for subsequent active and passive beamforming design.

Spectral efficiency  $R$  for downlink data transmission against the number of dominant paths  $L_s$  is shown in Fig. 4, where the ideal estimation and perfect feedback of DPGI are temporarily assumed here (i.e. the accurate DPGI is available at BS, and the scenario of non-ideal estimation and limited feedback is considered in the following simulations). We observe that although the achievable  $R$  of our proposed path selection (denoted as ‘Selected Paths’) is smaller than that of optimal path selection (obtained by exhaustive search, denoted as ‘Optimal Paths’), it is better than that of random path selection (denoted as ‘Random Paths’). In addition, when dominant paths are selected according to our proposed scheme, compared with the beamforming in [7] with partial random PGI, our proposed scheme in Subsection III-C achieves higher spectral efficiency  $R$ .

As shown in Fig. 5, when the quantized estimate of PGI is used for the beamforming design proposed in [7] (corresponding to lines with  $T = L = 6$  and  $T = 24$ ), higher spectral efficiency  $R$  can be achieved by adopting our proposed estimator rather than adopting MMSE estimator

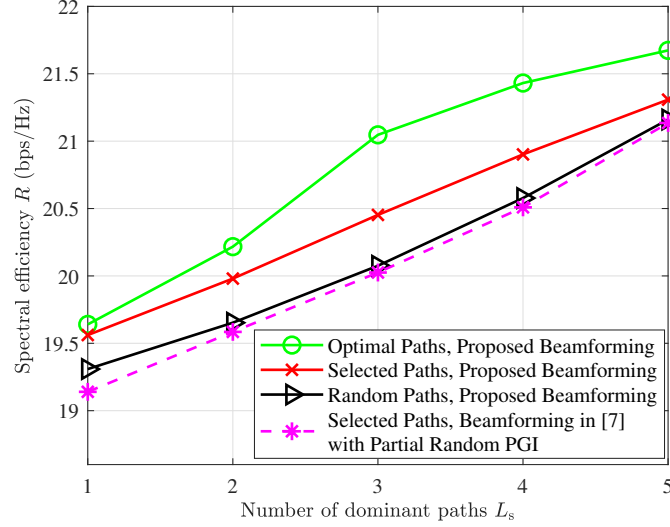


Fig. 4. Spectral efficiency  $R$  for downlink data transmission against number of dominant paths  $L_s$  when  $N_B = N_{B,v} \times N_{B,h} = 4 \times 4$ ,  $N_R = N_{R,v} \times N_{R,h} = 16 \times 16$ ,  $L = L_{RB} \times L_{RU} = 2 \times 3$ .

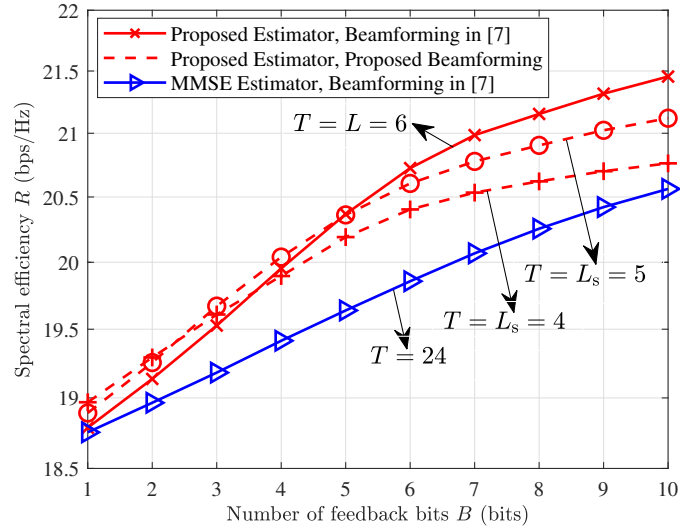


Fig. 5. Spectral efficiency  $R$  for downlink data transmission against number of feedback bits  $B$  when  $N_B = N_{B,v} \times N_{B,h} = 4 \times 4$ ,  $N_R = N_{R,v} \times N_{R,h} = 16 \times 16$ ,  $L = L_{RB} \times L_{RU} = 2 \times 3$ , PNR = -15 dB, DNR = 0 dB.

because of advantages of our proposed estimator in terms of estimation accuracy and feedback length. Besides, when the quantized estimate of DPGI is used for our proposed beamforming scheme (corresponding to lines with  $T = L_s = 5$  and  $T = L_s = 4$ ), although there is a certain performance loss in achievable spectral efficiency  $R$  compared with aforementioned scheme



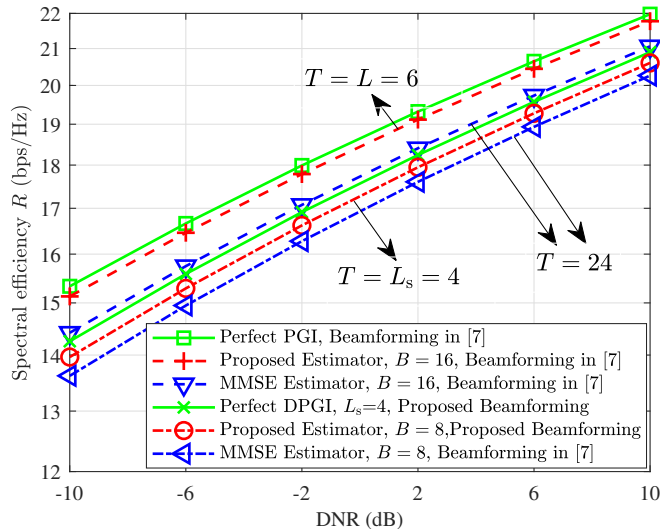


Fig. 6. Spectral efficiency  $R$  for downlink data transmission against DNR when  $N_B = N_{B,v} \times N_{B,h} = 4 \times 4$ ,  $N_R = N_{R,v} \times N_{R,h} = 16 \times 16$ ,  $L = L_{RB} \times L_{RU} = 2 \times 3$ ,  $L_s = 4$ ,  $\text{PNR} = -15$  dB.

using the whole PGI (corresponding to line with  $T = L = 6$ ), higher spectral efficiency  $R$  can be achieved around when  $B \leq 4$ . This is because when the number of feedback bits  $B$  is fixed, the accuracy of DPGI fed back to the BS increases with the decrease of feedback length  $T$ , which further leads to a corresponding increase of spectral efficiency  $R$ . Hence, the significance and superiority of our proposed path selection strategy are effectively demonstrated.

All the achievable spectral efficiency  $R$  under different settings increases exponentially with DNR as shown in Fig. 6. For the scenario where the whole PGI is exploited, the maximum  $R$  can be achieved when perfect PGI (ideal PGI estimation and perfect feedback) is used for beamforming proposed in [7]. In this case, the spectral efficiency gap can be controlled within 0.3 bps/Hz by exploiting our proposed estimator and a 16-bit RVQ codebook (corresponding to line with  $T = L = 6$ ). Besides, by exploiting our proposed path selection and beamforming scheme, the maximum  $R$  is achieved with perfect DPGI (ideal DPGI estimation and perfect feedback). In this case, by adopting our proposed estimator and a 8-bit RVQ codebook (corresponding to line with  $T = L_s = 4$ ), the spectral efficiency gap is also controlled within 0.3 bps/Hz. In addition, it can be seen that the spectral efficiency performance of our proposed estimator is much better than the spectral efficiency performance of the conventional MMSE estimator.

## V. CONCLUSIONS

In this paper, a path selection based feedback reduction and partial CSI-based beamforming scheme was proposed for the FDD RIS-assisted systems. Specifically, downlink PAI was first acquired at BS via the angle reciprocity. Then, we proposed a path selection strategy by removing the path with minimal contribution to spectral efficiency sequentially, during which the active and passive beamformers are alternatively optimized. Moreover, a DPGI estimation and feedback scheme is proposed, where both the length of downlink pilot signals and feedback vector are reduced to the number of selected dominant paths. Finally, the spectral efficiency of downlink data transmission is further improved by updating the active and passive beamformers based on the quantized estimate of DPGI. From the numerical experiments, we could observe the performance gain of proposed algorithms over the conventional schemes. More relevant cases may be further considered in the future work, e.g. the UE equipped with multiple antennas and the multi-user case in FDD RIS-assisted communication systems.

### APPENDIX A

#### PROOF OF LEMMA 1

According to the channel decomposition in (18), the objective function in (20) can be given by [25]

$$\mathbb{E} \left[ |\mathbf{h}^H \mathbf{f}_t|^2 \right] = \mathbb{E} \left[ \left| \mathbf{g}_r^T \mathbf{A}_r^H \mathbf{V} \mathbf{g}_s^* + \mathbf{g}_s^T \mathbf{A}_s^H \mathbf{V} \mathbf{g}_s^* \right|^2 \right] \quad (74)$$

$$= \mathbb{E} \left[ \left| \mathbf{g}_r^T \mathbf{A}_r^H \mathbf{V} \mathbf{g}_s^* \right|^2 \right] + \mathbb{E} \left[ \left| \mathbf{g}_s^T \mathbf{A}_s^H \mathbf{V} \mathbf{g}_s^* \right|^2 \right] \quad (75)$$

$$= \mathbb{E} \left[ \left| \mathbf{g}_s^T \mathbf{W}_s \mathbf{g}_s^* \right|^2 \right] + \mathbb{E} \left[ \left| \mathbf{g}_r^T \mathbf{W}_r \mathbf{g}_r^* \right|^2 \right], \quad (76)$$

where (75) is derived according to  $\mathbb{E} \left[ \mathbf{g}_s^* \mathbf{g}_r^T \right] = \mathbf{0}_{L_s \times L_r}$ , since  $\mathbb{E} \left[ g_{s,i}^* g_{r,j} \right] = \mathbb{E} \left[ \alpha_p^* \beta_q^* \alpha_m \beta_n \right] = \mathbb{E} \left[ \alpha_p^* \alpha_m \right] \mathbb{E} \left[ \beta_q^* \beta_n \right] = 0$  for  $\forall i = (q-1)L_{\text{RB}} + p \in \Lambda_s$  and  $\forall j = (n-1)L_{\text{RB}} + m \in \Lambda_r$  satisfying  $\{p, q\} \neq \{m, n\}$ . Besides,  $\mathbf{W}_s = \mathbf{A}_s^H \mathbf{V} \in \mathbb{C}^{L_s \times L_s}$  and  $\mathbf{W}_r = \mathbf{A}_r^H \mathbf{V} \in \mathbb{C}^{L_r \times L_r}$  are defined in (76) for simplicity. Here we respectively redefine variables  $i$  and  $j$  corresponding to values of the  $l_i$ -th element and the  $l_j$ -th element in  $\Lambda_s$ , where  $1 \leq i, j \leq L$ ,  $1 \leq l_i, l_j \leq L_s$ . Variables  $i$  and  $j$  also denote the indices of selected dominant cascaded paths, where we assume  $i = (q-1)L_{\text{RB}} + p$

and  $j = (n - 1)L_{\text{RB}} + m$ . The first term in (76) is further given by [25]

$$\mathbb{E} \left[ \left| \mathbf{g}_s^T \mathbf{W}_s \mathbf{g}_s^* \right|^2 \right] = \mathbb{E} \left[ \left| \sum_{l_i=1}^{L_s} \sum_{l_j=1}^{L_s} \mathbf{W}_s^{l_i, l_j} g_{s, l_i} g_{s, l_j}^* \right|^2 \right] = \mathbb{E} \left[ \left| \sum_{i \in \Lambda_s} \mathbf{W}_s^{l_i, l_i} |g_{s, l_i}|^2 + \sum_{i \neq j} \mathbf{W}_s^{l_i, l_j} g_{s, l_i} g_{s, l_j}^* \right|^2 \right] \quad (77)$$

$$= \mathbb{E} \left[ \left| \sum_{i \in \Lambda_s} \mathbf{W}_s^{l_i, l_i} |g_{s, l_i}|^2 \right|^2 \right] + \mathbb{E} \left[ \left| \sum_{i \neq j} \mathbf{W}_s^{l_i, l_j} g_{s, l_i} g_{s, l_j}^* \right|^2 \right] \quad (78)$$

$$= \sum_{i \in \Lambda_s} |\mathbf{W}_s^{l_i, l_i}|^2 \mathbb{E} [|g_{s, l_i}|^4] + \sum_{i \neq j} (\mathbf{W}_s^{l_i, l_i})^* \mathbf{W}_s^{l_j, l_j} \mathbb{E} [|g_{s, l_i}|^2 |g_{s, l_j}|^2] \\ + \sum_{i \neq j} |\mathbf{W}_s^{l_i, l_j}|^2 \mathbb{E} [|g_{s, l_i}|^2 |g_{s, l_j}|^2], \quad (79)$$

where (78) is due to  $\mathbb{E} [g_{s, l_i} g_{s, l_j}^*] = 0$  for  $\forall l_i \neq l_j$ . Then, we have

$$\mathbb{E} [|g_{s, l_i}|^4] = \mathbb{E} [|\alpha_p|^4] \mathbb{E} [|\beta_q|^4] = \left( (\mathbb{E} [|\alpha_p|^2])^2 + \mathbb{D} [|\alpha_p|^2] \right) \left( (\mathbb{E} [|\beta_q|^2])^2 + \mathbb{D} [|\beta_q|^2] \right) \\ = (1^2 + 1) \times (1^2 + 1) = 4, \quad (80)$$

and

$$\mathbb{E} [|g_{s, l_i}|^2 |g_{s, l_j}|^2] = \mathbb{E} [|\alpha_p|^2 |\alpha_m|^2 |\beta_q|^2 |\beta_n|^2], \quad (81)$$

where

$$\mathbb{E} [|\alpha_p|^2 |\alpha_m|^2] = \begin{cases} \mathbb{E} [|\alpha_p|^4] = (\mathbb{E} [|\alpha_p|^2])^2 + \mathbb{D} [|\alpha_p|^2] = 1^2 + 1 = 2, & \text{for } p = m \\ \mathbb{E} [|\alpha_p|^2] \mathbb{E} [|\alpha_m|^2] = 1 \times 1 = 1, & \text{for } p \neq m \end{cases}, \\ \mathbb{E} [|\beta_q|^2 |\beta_n|^2] = \begin{cases} \mathbb{E} [|\beta_q|^4] = (\mathbb{E} [|\beta_q|^2])^2 + \mathbb{D} [|\beta_q|^2] = 1^2 + 1 = 2, & \text{for } q = n \\ \mathbb{E} [|\beta_q|^2] \mathbb{E} [|\beta_n|^2] = 1 \times 1 = 1, & \text{for } q \neq n \end{cases}. \quad (82)$$

For a given cascaded path index  $i = (q - 1)L_{\text{RB}} + p$  with a combination  $\{p, q\}$ , the remaining  $(L - 1)$  optional indices of  $j = (n - 1)L_{\text{RB}} + m$  with a combination  $\{m, n\}$  can be divided into three types: *i*) The number of optional indices satisfying  $(p \neq m) \cap (q = n)$  is equal to  $(L_{\text{RB}} - 1)$ ; *ii*) The number of optional indices satisfying  $(p = m) \cap (q \neq n)$  is equal to  $(L_{\text{RU}} - 1)$ ; *iii*) The number of optional indices satisfying  $(p \neq m) \cap (q \neq n)$  is equal to  $(L - L_{\text{RB}} - L_{\text{RU}} + 1)$ . Therefore, based on (82), the closed-form expression of (81) is given by

$$\mathbb{E} [|\alpha_p|^2 |\alpha_m|^2 |\beta_q|^2 |\beta_n|^2] = \frac{2(L_{\text{RB}} - 1) + 2(L_{\text{RU}} - 1) + (L - L_{\text{RB}} - L_{\text{RU}} + 1)}{L_{\text{RB}} L_{\text{RU}} - 1} = \frac{L + L_{\text{RB}} + L_{\text{RU}} - 3}{L - 1}. \quad (83)$$

By substituting (80) and (83) into (79), we get

$$\begin{aligned} \mathbb{E} \left[ \left| \mathbf{g}_s^T \mathbf{W}_s \mathbf{g}_s^* \right|^2 \right] &= 4 \sum_{l_s=1}^{L_s} \left| \mathbf{W}_s^{l_s, l_s} \right|^2 + Q \sum_{l_i \neq l_j}^{L_s} \left( \mathbf{W}_s^{l_i, l_i} \right)^* \mathbf{W}_s^{l_j, l_j} + Q \sum_{l_i \neq l_j}^{L_s} \left| \mathbf{W}_s^{l_i, l_j} \right|^2 \\ &= (4 - 2Q) \|\text{diag}(\mathbf{W}_s)\|^2 + Q |\text{tr}(\mathbf{W}_s)|^2 + Q \|\mathbf{W}_s\|_{\text{F}}^2, \end{aligned} \quad (84)$$

where we define  $Q = \frac{L+L_{\text{RB}}+L_{\text{RU}}-3}{L-1}$ . Similarly, the second term in (76) is calculated as

$$\mathbb{E} \left[ \left| \mathbf{g}_r^T \mathbf{W}_r \mathbf{g}_r^* \right|^2 \right] = Q \sum_{l_r=1}^{L_r} \sum_{l_s=1}^{L_s} \left| \mathbf{W}_r^{l_r, l_s} \right|^2 = Q \|\mathbf{W}_r\|_{\text{F}}^2. \quad (85)$$

Finally, the expression of  $\mathbb{E} \left[ \left| \mathbf{h}^H \mathbf{f}_t \right|^2 \right]$  in Lemma 1 is obtained by combining (84) and (85).

## APPENDIX B

### PROOF OF LEMMA 2

For a given  $\mathbf{g}_s \in \mathbb{C}^{L_s \times 1}$ , the following equalities hold [25], [41]

$$\mathbb{E} \left[ \left| \mathbf{h}^H \mathbf{f}_t \right|^2 \right] = \mathbb{E} \left[ \left| \mathbf{g}_r^T \mathbf{A}_r^H \mathbf{f}_t \right|^2 \right] + \left| \mathbf{g}_s^T \mathbf{A}_s^H \mathbf{f}_t \right|^2 \quad (86)$$

$$= \mathbb{E} \left[ \mathbf{f}_t^H \mathbf{A}_r \mathbf{g}_r^* \mathbf{g}_r^T \mathbf{A}_r^H \mathbf{f}_t \right] + \left| \mathbf{g}_s^T \mathbf{A}_s^H \mathbf{f}_t \right|^2 \quad (87)$$

$$= \mathbf{f}_t^H \mathbf{A}_r \mathbb{E} \left[ \mathbf{g}_r^* \mathbf{g}_r^T \right] \mathbf{A}_r^H \mathbf{f}_t + \left| \mathbf{g}_s^T \mathbf{A}_s^H \mathbf{f}_t \right|^2, \quad (88)$$

where (86) is derived according to the channel decomposition in (18). Here we redefine variables  $i = (q-1)L_{\text{RB}} + p \in \Lambda_r$  and  $j = (n-1)L_{\text{RB}} + m \in \Lambda_r$ . Then, we have

$$\mathbb{E} \left[ g_{r,i}^* g_{r,j} \right] = \mathbb{E} \left[ \alpha_p^* \alpha_m \right] \mathbb{E} \left[ \beta_q^* \beta_n \right] = \begin{cases} 1, & \text{for } i = j, \{p, q\} = \{m, n\} \\ 0, & \text{for } i \neq j, \{p, q\} \neq \{m, n\} \end{cases}, \quad (89)$$

and further we get  $\mathbb{E} \left[ \mathbf{g}_r^* \mathbf{g}_r^T \right] = \mathbf{I}_{L_r}$ . Finally, the objective function in (86) can be formulated as

$$\mathbb{E} \left[ \left| \mathbf{h}^H \mathbf{f}_t \right|^2 \right] = \mathbf{f}_t^H \mathbf{A}_r \mathbf{A}_r^H \mathbf{f}_t + \left| \mathbf{g}_s^T \mathbf{A}_s^H \mathbf{f}_t \right|^2 = \|\mathbf{A}_r^H \mathbf{f}_t\|^2 + \left| \mathbf{g}_s^T \mathbf{A}_s^H \mathbf{f}_t \right|^2. \quad (90)$$

Thus proof is completed.

## REFERENCES

- [1] Y. Liu, X. Liu, X. Mu, T. Hou, J. Xu, M. Di Renzo, and N. Al-Dhahir, "Reconfigurable intelligent surfaces: Principles and opportunities," *IEEE Commun. Surveys Tuts.*, vol. 23, no. 3, pp. 1546–1577, Jul. 2021.
- [2] L. Dai, B. Wang, M. Wang, X. Yang, J. Tan, S. Bi, S. Xu, F. Yang, Z. Chen, M. D. Renzo, C.-B. Chae, and L. Hanzo, "Reconfigurable intelligent surface-based wireless communications: Antenna design, prototyping, and experimental results," *IEEE Access*, vol. 8, pp. 45 913–45 923, 2020.

- [3] W. Tang, J. Y. Dai, M. Z. Chen, K.-K. Wong, X. Li, X. Zhao, S. Jin, Q. Cheng, and T. J. Cui, "MIMO transmission through reconfigurable intelligent surface: System design, analysis, and implementation," *IEEE J. Sel. Areas Commun.*, vol. 38, no. 11, pp. 2683–2699, Nov. 2020.
- [4] S. Gong, C. Xing, X. Zhao, S. Ma, and J. An, "Unified IRS-aided MIMO transceiver designs via majorization theory," *IEEE Trans. Signal Process.*, vol. 69, pp. 3016–3032, 2021.
- [5] Z. Wang, L. Liu, and S. Cui, "Channel estimation for intelligent reflecting surface assisted multiuser communications: Framework, algorithms, and analysis," *IEEE Trans. Wireless Commun.*, vol. 19, no. 10, pp. 6607–6620, Oct. 2020.
- [6] C. Huang, A. Zappone, G. C. Alexandropoulos, M. Debbah, and C. Yuen, "Reconfigurable intelligent surfaces for energy efficiency in wireless communication," *IEEE Trans. Wireless Commun.*, vol. 18, no. 8, pp. 4157–4170, Aug. 2019.
- [7] Q. Wu and R. Zhang, "Intelligent reflecting surface enhanced wireless network via joint active and passive beamforming," *IEEE Trans. Wireless Commun.*, vol. 18, no. 11, pp. 5394–5409, Nov. 2019.
- [8] Y. Han, W. Tang, S. Jin, C.-K. Wen, and X. Ma, "Large intelligent surface-assisted wireless communication exploiting statistical CSI," *IEEE Trans. Veh. Technol.*, vol. 68, no. 8, pp. 8238–8242, Aug. 2019.
- [9] S. Gong, Z. Yang, C. Xing, J. An, and L. Hanzo, "Beamforming optimization for intelligent reflecting surface-aided SWIPT IoT networks relying on discrete phase shifts," *IEEE Internet Things J.*, vol. 8, no. 10, pp. 8585–8602, May 2021.
- [10] X. Xu, S. Zhang, F. Gao, and J. Wang, "Sparse Bayesian learning based channel extrapolation for RIS assisted MIMO-OFDM," *IEEE Trans. Commun.*, vol. 70, no. 8, pp. 5498–5513, Aug. 2022.
- [11] Y. Lin, S. Jin, M. Matthaiou, and X. You, "Tensor-based algebraic channel estimation for hybrid IRS-assisted MIMO-OFDM," *IEEE Trans. Wireless Commun.*, vol. 20, no. 6, pp. 3770–3784, Jun. 2021.
- [12] W. Tang, X. Chen, M. Z. Chen, J. Y. Dai, Y. Han, S. Jin, Q. Cheng, G. Y. Li, and T. J. Cui, "On channel reciprocity in reconfigurable intelligent surface assisted wireless networks," *IEEE Wireless Commun.*, vol. 28, no. 6, pp. 94–101, Dec. 2021.
- [13] D. Shen and L. Dai, "Channel feedback for reconfigurable intelligent surface assisted wireless communications," in *Proc. GLOBECOM IEEE Global Commun. Conf.*, Dec. 2020, pp. 1–5.
- [14] W. Tang, M. Z. Chen, X. Chen, J. Y. Dai, Y. Han, M. DiRenzo, Y. Zeng, S. Jin, Q. Cheng, and T. J. Cui, "Wireless communications with reconfigurable intelligent surface: Path loss modeling and experimental measurement," *IEEE Trans. Wireless Commun.*, vol. 20, no. 1, pp. 421–439, Jan. 2021.
- [15] C. Hu, L. Dai, S. Han, and X. Wang, "Two-timescale channel estimation for reconfigurable intelligent surface aided wireless communications," *IEEE Trans. Commun.*, vol. 69, no. 11, pp. 7736–7747, Nov. 2021.
- [16] H. Liu, J. Zhang, Q. Wu, H. Xiao, and B. Ai, "ADMM based channel estimation for RISs aided millimeter wave communications," *IEEE Commun. Lett.*, vol. 25, no. 9, pp. 2894–2898, Sep. 2021.
- [17] J. Chen, Y.-C. Liang, H. V. Cheng, and W. Yu, "Channel estimation for reconfigurable intelligent surface aided multi-user MIMO systems," Dec. 2019. [Online]. Available: <https://arxiv.org/abs/1912.03619>
- [18] X. Wei, D. Shen, and L. Dai, "Channel estimation for RIS assisted wireless communications-Part II: An improved solution based on double-structured sparsity," *IEEE Commun. Lett.*, vol. 25, no. 5, pp. 1403–1407, May 2021.
- [19] Y. Liu, S. Zhang, F. Gao, J. Tang, and O. A. Dobre, "Cascaded channel estimation for RIS assisted mmWave MIMO transmissions," *IEEE Wireless Commun. Lett.*, vol. 10, no. 9, pp. 2065–2069, Sep. 2021.
- [20] Z. Zhou, N. Ge, Z. Wang, and L. Hanzo, "Joint transmit precoding and reconfigurable intelligent surface phase adjustment: A decomposition-aided channel estimation approach," *IEEE Trans. Commun.*, vol. 69, no. 2, pp. 1228–1243, Feb. 2021.
- [21] P. Wang, J. Fang, H. Duan, and H. Li, "Compressed channel estimation and joint beamforming for intelligent reflecting surface-assisted millimeter wave systems," *IEEE Signal Process. Lett.*, vol. 27, pp. 905–909, May 2020.

- [22] X. Luo, "Multiuser massive MIMO performance with calibration errors," *IEEE Trans. Wireless Commun.*, vol. 15, no. 7, pp. 4521–4534, Jul. 2016.
- [23] D. Shen and L. Dai, "Dimension reduced channel feedback for reconfigurable intelligent surface aided wireless communications," *IEEE Trans. Commun.*, vol. 69, no. 11, pp. 7748–7760, Nov. 2021.
- [24] W. Chen, C.-K. Wen, X. Li, and S. Jin, "Adaptive bit partitioning for reconfigurable intelligent surface assisted FDD systems with limited feedback," *IEEE Trans. Wireless Commun.*, vol. 21, no. 4, pp. 2488–2505, Sep. 2021.
- [25] S. Kim, J. W. Choi, and B. Shim, "Downlink pilot precoding and compressed channel feedback for FDD-based cell-free systems," *IEEE Trans. Wireless Commun.*, vol. 19, no. 6, pp. 3658–3672, Jun. 2020.
- [26] S. Kim, J. W. Choi, and B. Shim, "Feedback reduction for beyond 5G cellular systems," in *Proc. IEEE Int. Conf. Commun. (ICC)*, May 2019, pp. 1–6.
- [27] X. Ge, W. Shen, C. Xing, L. Zhao, and J. An, "Training beam design for channel estimation in hybrid mmWave MIMO systems," *IEEE Trans. Wireless Commun.*, vol. 21, no. 9, pp. 7121–7134, Sept. 2022.
- [28] S. Gong, C. Xing, V. K. N. Lau, S. Chen, and L. Hanzo, "Majorization-minimization aided hybrid transceivers for MIMO interference channels," *IEEE Trans. Signal Process.*, vol. 68, pp. 4903–4918, 2020.
- [29] P. Cai, J. Zong, X. Luo, Y. Zhou, S. Chen, and H. Qian, "Downlink channel tracking for intelligent reflecting surface-aided FDD MIMO systems," *IEEE Trans. Veh. Technol.*, vol. 70, no. 4, pp. 3341–3353, Apr. 2021.
- [30] H. Zhou, S. Li, Y.-C. Liang, and L. Zhao, "Reconfigurable intelligent surface for FDD systems: Design and optimization," in *Proc. IEEE Int. Conf. Commun. (ICC)*, May 2022, pp. 2022–2027.
- [31] B. Guo, C. Sun, and M. Tao, "Two-way passive beamforming design for RIS-aided FDD communication systems," in *Proc. IEEE Wireless Commun. Netw. Conf. (WCNC)*, May 2021, pp. 1–6.
- [32] A. Papazafeiropoulos, P. Kourtessis, K. Ntontin, and S. Chatzinotas, "Joint spatial division and multiplexing for FDD in intelligent reflecting surface-assisted massive MIMO systems," *IEEE Trans. Veh. Technol.*, early access, Jun. 30, 2022, doi=10.1109/TVT.2022.3187656.
- [33] W. Chen, C.-K. Wen, X. Li, M. Matthaiou, and S. Jin, "Channel customization for limited feedback in RIS-assisted FDD systems," *IEEE Trans. Wireless Commun.*, early access, Dec. 08, 2022, doi=10.1109/TWC.2022.3226442.
- [34] W. Shen, L. Dai, B. Shim, Z. Wang, and R. W. Heath, "Channel feedback based on AoD-adaptive subspace codebook in FDD massive MIMO systems," *IEEE Trans. Commun.*, vol. 66, no. 11, pp. 5235–5248, Nov. 2018.
- [35] S. M. Kay, *Fundamentals of Statistical Signal Processing: Estimation Theory*. Prentice-Hall, Inc. Upper Saddle River, NJ, USA, 1993.
- [36] C. Xing, S. Wang, S. Chen, S. Ma, H. V. Poor, and L. Hanzo, "Matrix-monotonic optimization Part II: Multi-variable optimization," *IEEE Trans. Signal Process.*, vol. 69, pp. 179–194, 2020.
- [37] F. Gao, B. Wang, C. Xing, J. An, and G. Y. Li, "Wideband beamforming for hybrid massive MIMO terahertz communications," *IEEE J. Sel. Areas Commun.*, vol. 39, no. 6, pp. 1725–1740, Jun. 2021.
- [38] C. Xing, S. Wang, S. Chen, S. Ma, H. V. Poor, and L. Hanzo, "Matrix-monotonic optimization Part I: Single-variable optimization," *IEEE Trans. Signal Process.*, vol. 69, pp. 738–754, 2020.
- [39] P.-A. Absil, R. Mahony, and R. Sepulchre, *Optimization algorithms on matrix manifolds*. Princeton, NJ, USA: Princeton Univ. Press, 2009.
- [40] C. Xing, S. Ma, and Y. Zhou, "Matrix-monotonic optimization for MIMO systems," *IEEE Trans. Signal Process.*, vol. 63, no. 2, pp. 334–348, Jan. 2015.
- [41] S. Kim and B. Shim, "Energy-efficient millimeter-wave cell-free systems under limited feedback," *IEEE Trans. Commun.*, vol. 69, no. 6, pp. 4067–4082, Jun. 2021.